Flexibility improvement of 1000 MW ultra-supercritical unit under full operating conditions by error-based ADRC and fast pigeon-inspired optimizer

Guolian Hou [a], Ting Huang [a], Congzhi Huang [a,b,*]

[a] *School of Control and Computer Engineering, North China Electric Power University, Beijing, 102206, China*
[b] *Key Laboratory of Power Station Energy Transfer Conversion and System, North China Electric Power University, Beijing, 102206, China*

A B S T R A C T

The flexible operation capacity of ultra-supercritical (USC) unit under full operating conditions must be promoted to adapt a larger-scale renewable energy integrated into the power grid. To this end, a flexible operation method fusing the error-based ADRC and fast pigeon-inspired optimizer is designed and employed to USC unit to achieve deep peak shaving and rapid load regulation. Firstly, the urgency of the proposed method is illustrated via analyzing the control difficulties of USC unit under flexibility requirements. Then, the error-based ADRC scheme which adopts a broader sense of disturbances in control loops is formulated for USC unit. Thanks to the error-based ADRC, all the unknown uncertainties in unit are precisely estimated and compensated in real-time which is conducive to its precise load regulation. Furthermore, the fast pigeon-inspired optimizer combined with the two-stage optimization and bi-quantum parallel search is used to attain the optimal parameters of error-based ADRC. A multi-criteria optimization function composes the load tracking error and smoothness of manipulated variable is established to guide the unit to flexible operation. The integrated control scheme effectively blends the features of rapid load tracking, exactly disturbance rejection and fast parameters tuning. Finally, the effectiveness of the proposed controller is successfully confirmed based on a 1000 MW USC unit. The simulation results reveal that the flexible operation capacity of USC unit under full operating conditions is promoted by the error-based ADRC approach. The average load tracking error of unit is reduced from 4.22 MW to 2.45 MW, and the settling time is simultaneously shortened from 188.52s to 158.80s compared to the ADRC method. Hence, the integrated error-based ADRC method provides a practical reference for the flexibility improvement of 1000 MW USC unit under full operating conditions.

1. Introduction

The large-scale application of renewable energy sources requires the thermal power unit to improve its operational flexibility to enhance the stability of the power grid [1–3]. Recently, the ultra-supercritical (USC) unit with high-temperature and high-pressure steam has become the main force in thermal power unit due to its high thermal efficiency and environmental friendliness [4,5]. Therefore, to accelerate the transformation of the low-carbon power system, the flexible operation capacity of USC unit under full operating conditions must be promoted.

The operational flexibility of USC unit refers to the ability to fast change output power in an affordable way for external load demand. In other words, the flexibility grade of USC unit depends on its deep peak shaving capability and load ramping rate [6,7]. The deep peak shaving ability represents how much space the USC unit can provide for the renewable energy resources in power grid. However, it is not easy for the conventional USC unit to achieve the flexible operation under full operating conditions. On one hand, the peak shaving capacity of USC unit is limited by the minimum stable firing rate of one-through boiler [8]. The pressure and temperature of the working medium in boiler fluctuate frequently when unit operating at a lower 35% rated load. Then, exorbitant steam temperature resulted by the excessive load ramping rate will cause device damagement. Various measures such as the control system upgrade, materials development and stable combustion technology at ultra-low rated load should be employed to ensure the operational safety of once-through boiler. On the other hand, due to the lack of drum in USC unit the load response speed is reduced and the

Nomenclature		ESO	extended state observer
		ω_o	observer bandwidth
Acronyms		ω_c	controller bandwidth
ADRC	active disturbance rejection control	b_0	input gain of controller
EADRC	error-based active disturbance rejection control	u_B	coal feeding rate (t/h)
USC	ultra-supercritical	μ_T	position of main steam valve (t/h)
T-S	Takagi-Sugeno	u_W	water feeding rate (t/h)
PSO	particle swarm optimization	N	active power (MW)
PIO	pigeon-inspired optimization	P_T	main steam pressure (MPa)
BQPIO	bi-quantum pigeon-inspired optimization	T	intermediate point temperature (°C)
ABC	artificial bee colony	RBL	boiler rated load
EPO	emperor penguin optimization	RCM	load ramping rate
AGC	automatic generation control		

load disturbance is increased. Frequent load fluctuations have exceeded the inherent regulation ability of the traditional USC unit which is not beneficial for its flexible operation under full operating conditions. Thus, flexibility renovations on USC unit are urgent.

With the flexible operation of supercritical coal-fired power unit becoming a research hotspot, achievements emerge in large numbers. They mainly focus on these four aspects, namely the modeling methods and devices materials development of once-through boiler, steam extraction and energy storage from steam turbine, the upgrading of coordinated control system and the cooperation of unit with renewable energy generation. In modeling, a fuzzy neural network modeling scheme combined with the fuzzy rules, k-means++ and supervised adaptive gradient descent algorithms was used to establish the model of 1000 MW USC unit to meet the operational stability requirements. The satisfactory modeling accuracy of the proposed algorithm was confirmed by simulation results [9]. To investigate the dynamics of the supercritical unit, a flexible modeling method integrated by T-S fuzzy modeling, automatic clustering and adaptive moth-flame optimization was put forward. The established model revealed the ideal identification precision within [30%BRL, 100%BRL]. Nevertheless, the covered load range still need to be enlarged [10]. Additionally, a multiple-process model optimized by the gray wolf optimizer was constructed for a cleaner supercritical power unit. That model covered all processes from ultra-low rated load to the maximum boiler continuous rating then to shutdown which laid a good foundation for the flexible operation of unit [11]. However, more comparisons were required to validate the parameters optimization performance of the gray wolf algorithm. To achieve the flexible and economic operation of a 660 MW direct air-cooling coal-fired power unit, the carbon capture was introduced and then a dynamic modeling of unit was presented. Results showed that the minimum power load of the unit was reduced by 44 MW and the ramping speed was improved by 3.75 MW min^{-1} [12]. A distributed-parameter model which made it possible to simulate the power boiler operation in the conditions of rapid load variations was proposed. Then, model suitability was successfully confirmed by various analyses [13]. However, the above-mentioned models were usually accompanied by enormous calculations and high-cost which is not conducive to industrial extension. Moreover, finding a new material that can withstand high-temperature and high-pressure to reform the devices in once-through boiler is also instrumental in the deep peak shaving capability promotion. Nanomaterial manufactured and used at a very small scale but with positive electrical and mechanical properties is considered as potential industrial application including oil refineries, petrochemical industries and buildings [14]. The latest research results revealed that the addition of Li_2SO_4 had positive effect on the thermal stability of polyvinyl alcohol-carbon based nanotubes based thin film composites [15]. Besides, the structural and dielectric properties of nanosized crystal X-type hexagonal ferrites could be tuned by the variations of Co and Zn [16]. These successful nanomaterials attempts

provided effective references for improving the deep peak shaving ability of boiler from material transformation. Nevertheless, new nanocomposites that can balance the mechanical, thermal stability, electrical and environmentally friendly properties still need to be developed [17]. Furthermore, the steam extraction renovation of steam turbine is an efficient way for unit to quickly change the output power. For the load flexibility improvement of power unit, a load regulation method based on the multi-scale energy storage utilization and combination of extraction throttling and feedwater bypass throttling was proposed. The flexible load regulation under different load command conditions was proved by results [18]. However, the energy storage characteristics of different feedwater heaters should be further analyzed. Furthermore, the condensate throttling strategy was also beneficial to the flexible operation of a 600 MW supercritical pure condensing unit [19] and a 350 MW cogeneration unit [20]. Five different measures were introduced to regulate the extraction steam of high-pressure heaters in a 660 MW supercritical coal-fired unit for operational flexibility. The thermal storage was validated as a feasible solution for the flexibility enhancement of unit [21]. Nevertheless, the control strategies and other influencing factors were not considered in the operational flexibility evaluation of the coal-fired unit. Then, an improved control model considering heat storage changes was presented for the flexible operation of double-reheat power unit. The load response speed of unit had been increased with the improved controller [22]. Additionally, the heat storage tank, electric boiler, high pressure-low pressure bypass heating [23] as well as the high back-pressure and the low-pressure turbine zero power output renovations [24] were successfully used to promote the peak shaving capacity of the cogeneration unit. Whereas, the valve safety was ignored in the regulation process of extraction steam. Besides, the energy storage technologies had not come to the industrial extension stage. Next, an integrated generation scheme combined with the power plant and solar thermal power was given to boost the unit to undertake peak-shaving tasks. The maximum load cycling rate of the 660 MW solar-aided coal-fired power unit was increased from 3.3 MW min^{-1} to 13.2/13.2/9.9 MW min^{-1} under sunny/light cloud cover/strong cloud cover cases, respectively [25]. Whereas, the coordinated control system matched with the integrated power generation technology still need to be investigated. Significantly, the coordinated control system upgrading which has a positive effect on the rapid flexibility promotion of power unit is favored by researchers due to its climate independence and low-cost. To enhance the coordinated control performance of a 1000 MW USC unit in flexible-operation mode, a novel nonlinear model predictive control approach combined with the input convex neural network was proposed. Results demonstrated that the fast and stable load tracking capacity of USC unit was obtained based on the improved control method [26]. The issue of reheat steam over temperature has limited the load ramping rate of the double-reheat USC unit. To solve this problem, a new coordinated control strategy assisted by high-pressure extraction steam throttling was presented and verified in

the flexible operation of unit [27]. However, the throttling loss was not taken into account which influences the operational economy of unit. Besides, an optimal control strategy integrated the stair-like predictive control, feedforward and decoupling control concepts was utilized to guarantee the operational flexibility, stability and economy of USC unit. Experiments showed its effectiveness but depended on the traditional control experience [28]. The load tracking capability of a drum boiler unit which considered the energy demand decoupling was effectively promoted by the generalized predictive control algorithm [29]. Additionally, both the energy-saving efficiency and control performance of a 1000 MW USC unit were enhanced via the energy-saving predictive control scheme [30]. Rapid and stable load response was acquired by the USC unit thanks to the affine nonlinear control method when fast load variations and frequency disturbances existed in power grid [31]. Nevertheless, how to make use of the above-mentioned complex or nonlinear control algorithms in the actual power generation process is still a significant problem to be solved. Especially, there are few existing solutions that can realize the flexible operation of 1000 MW USC unit under full operating conditions. Under these circumstances, the error-based active disturbance rejection control (EADRC) technology with remarkable control performance and industrial practicability is created and developed commendably. The EADRC has been proved to be a replacement for the industrial PID. Hence, a practical EADRC scheme is necessary for the flexible operation of USC unit under full operating conditions.

EADRC is an advanced control algorithm that commendably inherits and develops the prominent estimation and disturbance rejection performance as well as the strong robustness of traditional linear active disturbance rejection control (ADRC) [32–34]. With the gains of EADRC are bandwidthized, the parameters tuning problem is simplified. That effectively improves its industrial applicability [35,36]. Particularly, by directly regulating the error dynamics of closed loop in real-time, EADRC can efficiently deal with high-frequency uncertainties without the higher-order time-derivative of reference input. Additionally, EADRC enables a magnitude and/or rate limitation of the control signal as well as bumpless changes with the industrial controller. Based upon that, the EADRC with a fixed 1- degree-of freedom structure and model independence realizes a leap from theoretical research to engineering practice. A multi-agent EADRC scheme was effectively employed to enhance the flexible operation capacity of supercritical cogeneration unit. However, the stability of the reinforcement learning algorithm was hard to ensure that impacted the stable control performance of boiler-turbine unit [37]. In Ref. [38], the EADRC approach was successfully applied for pitch control of variable speed wind turbine to track the power reference on a 1.5 MW FAST simulator. To obtain the constant power generation of photovoltaics, the EADRC technology was used to improve the maximum power point tracking performance. Simulations demonstrated the capability of EADRC strategy in reference power tracking with a tracking error of 0.21% and settling time of 0.019s [39]. The flexible load control of coal-fired unit [40] and nuclear cogeneration unit [41] was achieved by the ADRC. However, the gains tuning by manual was time-consuming. The EADRC, feedforward and feedback-type disturbance observer were combined to constitute a hierarchical anti-disturbance control method and applied to the motion control of piezo-actuated nano positioner. The superior control performance of the proposed controller was confirmed [42]. An EADRC approach was designed to accomplish the trajectory tracking task, results verified its excellent tracking performance in vibration suppression [43]. The above effective applications adequately illustrated the extraordinary response speed, disturbance rejection ability and industrial practicability of EADRC. Against this background, employing the EADRC strategy to improve the deep peak shaving and rapid load regulation capacities of USC unit devoted to the flexible operation under full operating conditions is practical and forward-looking.

Parameters selections of EADRC play a key role on its control performance. In practice, the parameters of controllers are usually tuned by manual which is inefficient and time-consuming. Thus, an intelligent and convenient scheme for automatic parameter acquisition should be investigated. Swarm intelligent algorithms with the advantages of simple principle, extensive and accurate search ability are popular in the optimization field [44,45]. The quantum simultaneous whale optimization algorithm [46] was employed to minimize the operating costs in the energy field. Significant cost reduction was obtained by experiments. The particle swarm optimization (PSO) algorithm exhibited well in the efficient parameters extraction of photovoltaic models [47]. A hybrid artificial bee colony differential evolution optimizer was developed to accurately estimate the optimum parameters of the proton exchange membrane fuel cells model to reach accurate current/voltage curves [48]. However, the universality and convergence speed of the above-mentioned swarm intelligent algorithms had not been fully concerned. To this end, a novel two-stage optimization algorithm namely pigeon-inspired optimization (PIO) was proposed [49]. Inspired by the homing behavior of pigeons, the map and compass operator and the landmark operator constitute the two optimization stages of the PIO algorithm [50]. The PIO algorithm had been extensively applied because of its strong exploration and exploitation ability. The enhanced PIO algorithm with Taguchi method was presented to extract the optimal parameters of photovoltaic modules for maximum power point tracking and control. A stable maximum power tracking value at 5.15×10^3 W was achieved under 100% light, 80%, 60%, 40% and 20% by experimental calculations [51]. It is noted that the dimension setting and the orthogonal tables construction in Taguchi method still needs to be focused. Besides, the superiorities of hierarchical PIO [52] in the parameter estimation of maximum power point tracking method for photovoltaic systems were also verified. The multi-strategy PIO [53] and modified PIO [54] were also successfully employed to optimize the parameters of ADRC in unmanned aerial vehicles and mobile robots, respectively. Nevertheless, the convergence rate of the above improved PIO algorithm had become one of the most important factors restricting its application in practical optimization problems. For flexibility promotion, the optimal parameters of the fuzzy model of cogeneration unit under different heat-power coupling technologies were quickly attained by the bi-quantum pigeon-inspired optimization (BQPIO) algorithm [55]. It follows that the novel BQPIO algorithm is an extremely effective solver in the optimal parameter extraction of process model for power unit.

The motivation of this paper is to propose the practical EADRC scheme for the operational flexibility promotion of 1000 MW USC unit under full operating conditions. Wherein, the parameters choices of EADRC play a vital role in the load tracking performance of the USC unit. Besides, there are few applications of the BQPIO algorithm in the parameters optimization of EADRC, and its enough potential worth to be tapped. Consequently, further investigating the convergence speed and search precision of the BQPIO algorithm to quickly obtain the optimal parameters of EADRC can facilitate the flexible operation of USC unit.

To sum up, a practical EADRC scheme is constructed and employed to enhance the flexible operation capacity of 1000 MW USC unit under full operating conditions. The main contributions of this paper can be summarized as follows.

1) An industrially practical EADRC solution is presented for the flexible operation issue of a 1000 MW USC unit. In EADRC framework, all the unknown uncertainties include unmodeled dynamics and coal quality variations are intensively estimated and compensated in real-time which contributes to the flexible operation of USC unit.
2) The load tracking accuracy and smoothness of manipulate variables are considered in the multi-criteria objective function. Then, the fast BQPIO algorithm with desired industrial computing speed is used to obtain the optimal parameters of EADRC by minimizing the objective function. The transparent parameter optimization process enables the control performance of USC unit can always meet the flexibility requirements.

3) Based on the actual on-site data of 1000 MW USC unit, the effectiveness of the presented EADRC scheme is proved via comparative simulation experiments. Corresponding results indicate the ideal flexible operation capacity of USC unit under the wide load range from 30% BRL to 90% BRL.

The rest of this paper is organized as follows: in Section 2, the flexibility requirements of 1000 MW USC unit under full operating conditions are described. Afterwards, the details of the flexible EADRC approach, multi-criterion optimization objective and BQPIO algorithm are proposed in Section 3. Then, the simulation tests and evaluations on the rapid load regulation ability of the 1000 MW USC unit are illustrated in Section 4 to verify its operational flexibility under full operating conditions. Finally, conclusions and future research directions are discussed in Section 5.

2. Flexibility of the 1000 MW USC unit

2.1. Description of USC unit

The structural schematic diagram of 1000 MW USC unit and its simplified model is exhibited in Fig. 1. It can be seen that USC unit can be regarded as a huge and complex thermodynamic system consisted by two major subsystems namely the once-through boiler and steam turbine. Besides, the heat recovery system is used to supplement the boiler and turbine. The once-through boiler provides the heat for working medium by burning the coal. The heat is converted into mechanical energy in steam turbine and then to the electricity. Ulteriorly, the working process of the 1000 MW USC can be simply described as follows. Firstly, the feed water is heated in combustor with the energy from coal combustion and then passes through the water wall, separator and superheaters finally turned into the main steam. Afterwards, the high-temperature and high-pressure steam flows into the steam turbine to

drive the generator to produce electricity. In the end, the exhaust steam is condensed, deoxidized and heated in the heat recovery system and flows the economizer finally becomes the feed water for boiler. The multistage utilization of energy brings high thermal efficiency to the USC unit.

In summary, the shape and dynamic characteristics of working medium in once-through boiler are complicated and changeable. Considering the most significant factors in operating process and the convenience of controller designing, the USC unit can be simplified as a three-input three-output system illustrated in Fig. 1. The coal feeding rate (u_B, t/h), position of main steam valve (μ_T, %) and water feeding rate (u_W, t/h) are regarded as the input variables. The three output variables are active power (N, MW), main steam pressure (P_T, MPa) and intermediate point temperature (T, °C).

2.2. Flexibility requirements

Promoting the deep peak shaving and rapid load regulation abilities are the two main effective ways to achieve the flexible operation of USC unit under full operating conditions. To this end, a smaller load tracking error and shorter settling time are desired for USC unit during the load regulation. Besides, it is necessary for the USC unit to maintain the distinguished disturbance rejection performance, stable main steam pressure and intermediate point temperature. Meanwhile, smooth position of the main steam valve, coal feeding rate and water feeding rate are required to ensure the operational economy and safety of unit. However, restricted by the minimum steady burning rate of once-through boiler, a load ramping rate higher than 2.5% MCR/min is hard for the traditional USC unit to achieve when operating at a lower 35% rated load. Consequently, employing the practical EADRC technology to upgrade the control performance of USC unit for above-mentioned requirements attainment is benefit to the flexible operation under full operating conditions.
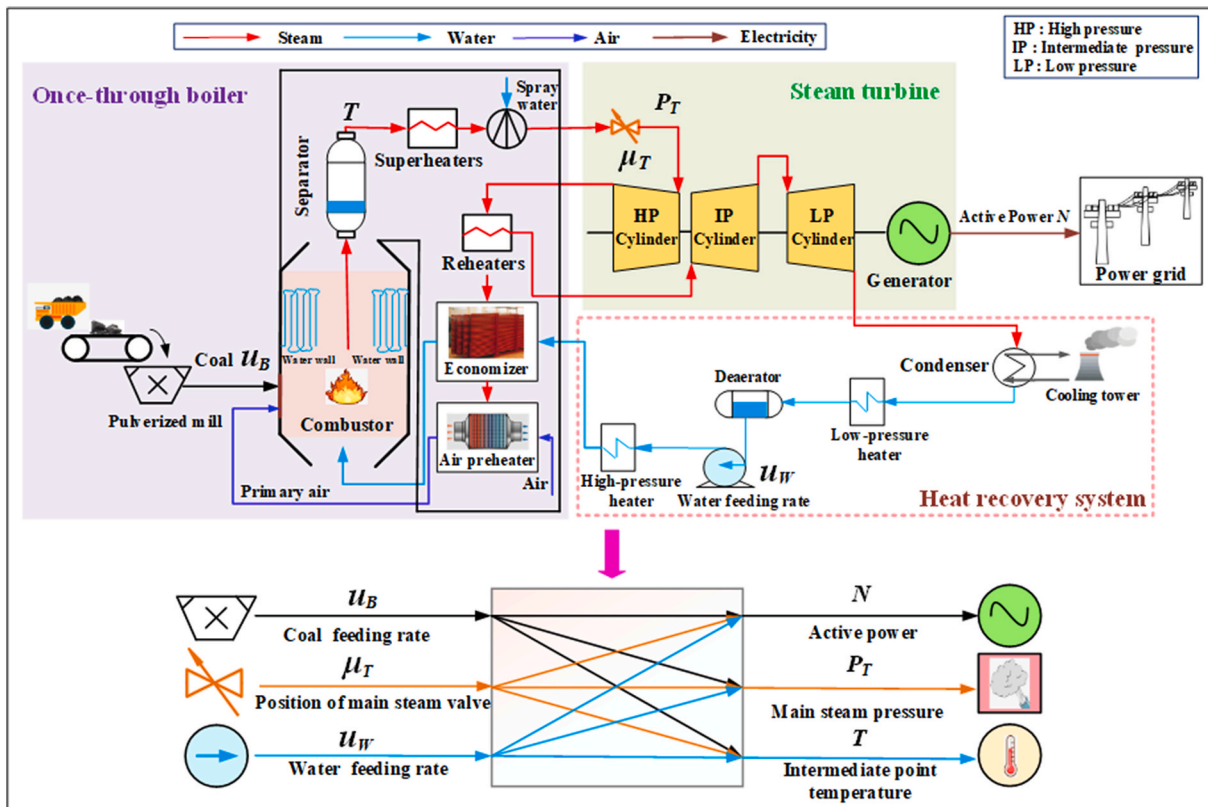

Fig. 1. Structural schematic diagram and corresponding simplified model of the 1000 MW USC unit.

3. Proposed flexible operation approach fusing the EADRC and BQPIO algorithm

The designing of the flexible EADRC approach shown in Fig. 2 for the USC unit contains two steps. First of all, EADRC1, EADRC2 and EADRC3 are assigned for the active power, main steam pressure and intermediate point temperature channels of USC unit, respectively. Afterwards, the fast BQPIO algorithm is used to automatically obtain the optimal parameters of EADRC. In EADRC, all the unknown uncertainties in the USC unit are regarded as a total disturbance. When appropriate parameters are selected for EADRC, the total disturbance is exactly estimated by

extended state observer (ESO) in real-time and then compensated by the state feedback control. Under these circumstances, the control performance of USC unit regulated by the flexible EADRC scheme can always meet the flexibility requirements.

3.1. Essentials of EADRC approach

With the rapid development of advanced control strategies, the control performance is not the only index to evaluate the effectiveness of a control strategy in actual industrial process. The industrial practicability of controller is important as well. Accordingly, the EADRC strategy
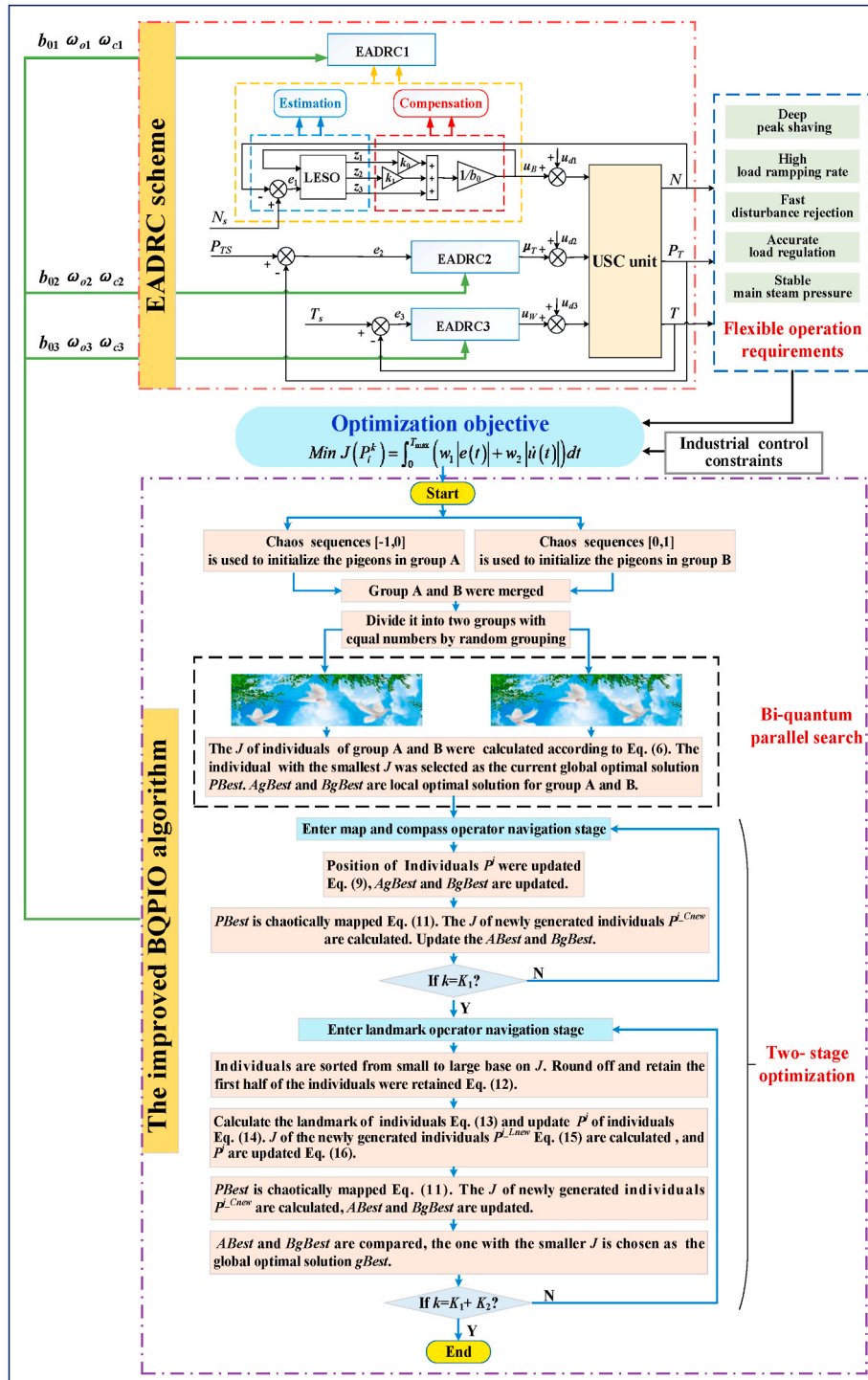

Fig. 2. Framework of the flexible EADRC approach for the 1000 MW USC unit.

which reaches a reasonable trade-off between the control performance and facilitation is instrumental in the operational flexibility improvement of USC unit under wide-load range. The EADRC1 for active power channel of USC unit is taken as an example to describe the principle of EADRC, others are similar.

Generally, the power generation process can be described as a second-order controlled process:

$$\ddot{N} = g(t, \cdots, u_{d1}) + bu_B \tag{1}$$

Where $\ddot{N}$ stands for the second-order derivative of active power in USC unit. g is the synthesis function of time variation t, external disturbance u_{d1} caused by the variation of environment and coal quality, etc. $b \neq 0$ is the high frequency uncertainties in USC unit. The estimation of b is noted as b_0. Define the total disturbance f as $f = g + (b - b_0)u_B$, including the unknown external disturbance and internal dynamics. The estimation of f is denoted as f^*.

The state variable matrix $\rho = [\rho_1 \; \rho_2 \; \rho_3] = [e_1 \; \dot{e}_1 \; f^*]$ is chosen in the designing of second-order Luenberger ESO in EADRC1. $\rho_3 = f^*$ is added as the expanded state of ESO. Then, the load tracking error of USC unit and its derivatives are defined as follows:

$$
\begin{aligned}
e_1 &= N_s - N = \rho_1 \\
\dot{e}_1 &= \dot{N}_s - \dot{N} = \dot{\rho}_1 = \rho_2 \\
\ddot{e}_{11} &= \ddot{N}_s - \ddot{N} = \ddot{\rho}_1 = \dot{\rho}_2 = \ddot{N}_s - f - b_0 \cdot u_B
\end{aligned}
\tag{2}
$$

Where N_s is the load demand from AGC. Evidently, the EADRC has a 1-degree-of freedom structure. The expansion state of Eq. (2) can be rewritten as:

$$
\begin{cases}
\dot{\rho}_1 = \rho_2 \\
\dot{\rho}_2 = \rho_3 - b_0 \cdot u_B \\
\dot{\rho}_3 = \dot{f}^*
\end{cases}
\tag{3}
$$

Where $\dot{f}^* = \ddot{N}_S - \dot{f}$. It's assumed here that f^* is time-differentiable and $\dot{f}^*$ is bounded. For the above system expressed in error-based form, the corresponding second-order ESO considered its model and assumed polynomial-type disturbance model can be formulated as:

$$
\begin{cases}
\dot{z}_1 = z_2 + l_1 \cdot e_1 \\
\dot{z}_2 = z_3 - b_0 \cdot u_B + l_2 \cdot e_1 \\
\dot{z}_3 = l_3 \cdot e_1
\end{cases}
\tag{4}
$$

Where $l = [l_1 \; l_2 \; l_3]$ is the pending gains of ESO. z_1, z_2 and z_3 are the outputs of ESO. The load tracking error e_1 and total disturbance f can be accurately estimated in real-time by ESO when the gains are appropriately set. Then, the state feedback control law is presented as a PD control law for USC unit to precisely response to the load demand N_S.

$$u_B = \frac{k_0 \cdot z_1 + k_1 \cdot z_2 + z_3}{b_0} \tag{5}$$

According to the stability analysis of EADRC, the choices of gains are as follows: $k_1 = 2\omega_c$, $l_1 = 3\omega_o - k_1$, $k_0 = \omega_c^2$, $l_2 = 3\omega_o^2 - l_1 k_1$, $l_3 = \omega_o^3$. Here, the ω_c and ω_o are the bandwidths of controller and observer, respectively. The larger observer bandwidth ω_o, the better the tracking performance of the extended states is. Then, the total disturbance including the high-frequency perturbations can be estimated and compensated more precisely by the controller. However, the increasing ω_o will lead to the amplifying of measurement noise. On the other hand, the parameters tuning problem of EADRC is greatly simplified by placing all the poles of controller at the same location $-\omega_c$. Stable control performance at lower-frequency can be improved by enlarging the desired controller bandwidth ω_c. Therefore, the tunings of ω_c and ω_o is a trade-off among the tracking performance, robustness and measurement noise sensitivity of EADRC in practice. The observer bandwidth ω_o is always wider than the controller bandwidth ω_c. A good rule of thumb is that $\omega_o \approx 3 \sim 5\omega_c$ [56]. An appropriate value must be arranged for b_0 according to the system since it scales the entire feedback control law thus significantly

influencing the tracking performance of controller. Based on the above theoretical derivation, the structure of second-order EADRC is illustrated in Fig. 3. The EADRC in the three output channels of USC unit has the same structure.

3.2. Parameters optimization problem of EADRC

To sum up, prominent control performance of EADRC strategy can be attained when its parameters ω_c, ω_o and b_0 are assigned with appropriate values. To satisfy the flexibility demands of USC unit under full operating conditions, J is chosen as the total objective function in the load response process. The optimization ranges of parameters are selected according to the empirical method. Thus, the EADRC parameters optimization problem is formulated as

$$Min \; J(P_i^k) = \int_0^{T_{max}} (w_1|e(t)| + w_2|\dot{u}(t)|)dt$$

$$
s.t. \begin{cases}
|e(t)| = \sum_{s=1}^{3} |e_s(t)| \\[2mm]
|\dot{u}(t)| = \sum_{s=1}^{3} |\dot{u}_s(t)| \\[2mm]
300 \text{ MW} \leq N \leq 1000 \text{ MW} \\[1mm]
65 \text{ t/h} \leq u_B \leq 390 \text{ t/h} \\[1mm]
750 \text{ t/h} \leq u_W \leq 2500 \text{ t/h} \\[1mm]
\mu_T \in \begin{cases} [35\%, 75\%], \text{ sliding pressure mode} \\ [75\%, 95\%], \text{ constant pressure mode} \end{cases} \\[3mm]
|\dot{u}(t)| \in (0, 0.1N_S] \\[1mm]
0.05 \leq b_{0s} \leq 50 \\[1mm]
0.05 \leq \omega_{os} \leq 50 \quad s = 1,2,3. \\[1mm]
0.05 \leq \omega_{cs} \leq 50
\end{cases}
\tag{6}
$$

Where P_i^k is the parameters matrix of EADRC scheme that is symbolized by the i-th individual in k-th iteration in the BQPIO algorithm. $\dot{u}(t)$ represents the smoothness of the manipulated variables in the USC unit during the load regulation process. The tracking error is noted as $e_s(t)$. w_1 and w_2 are the weight factors of sub-objective functions in the load response process. T_{max} is the maximum value of sampling time.

3.3. The two-stage BQPIO algorithm

The BQPIO algorithm mainly contains four improvements that contribute to the remarkable search accuracy and convergence speed, namely the two-stage optimization, bi-quantum population, parallel optimization and chaotic mapping. The two-stage optimization and chaotic mapping bring out the remarkable search precision of BQPIO algorithm by effectively avoiding the pigeons falling into the local optimal solution. Besides, the bi-quantum population and parallel optimization characteristics of the BQPIO algorithm accelerate the pigeons approach to the global optimal solution. Then, considering the important influence of parameter selections on the control performance of EADRC, the BQPIO algorithm is used to quickly obtain the optimal parameters of EADRC scheme to achieve the flexible operation of USC unit covered wide-load range. The two-stage homing behavior consisted by map and compass navigation and landmark navigation enabling pi-
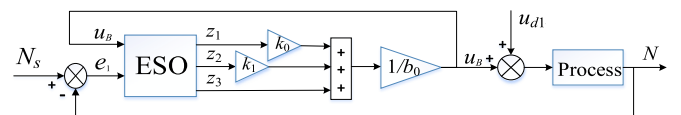

Fig. 3. Structure of the second-order EADRC1.

geons to fast find their nest. In the initial stage of pigeons' homing, the individual with the minimum fitness will be considered as the initial position of the pigeon nest. Then, other individuals approach to the pigeon nest. Each individuals of pigeon groups represents a parameter matrix of EADRC. The global optimal individual is selected as the location of the pigeon nest which is also the optimal parameters of EADRC. The details of the BQPIO algorithm are described as follows.

Step 1. Two opposite sequences [-1,0] and [0,1] are used to initialize the individuals in two populations A and B respectively. Thus, individuals can traverse the solution space of [-1,1] to search for precise solution.

$$G_j(i+1) = \varphi \cdot G_j(i) \cdot [1 - G_j(i)] \quad (i=1,2,\cdots,M; j=1,2) \tag{7}$$

Where φ is selected as 4. All individuals are in the state of complete chaotic. $G_1(1)$, $G_2(1) \in rand(-1,0)$, M is the population size.

Based on the logistic chaotic sequence Eq. (7), the positions of individuals in two populations are initialized:

$$P_i^j(0) = P^{min} + G_j(i) \cdot (P^{max} - P^{min}) \quad (i=1,2,\cdots,M; j=1,2) \tag{8}$$

where $P_i^j(0)$ is the initial position of i-th individual in the j-th pigeon population. P^{max} and P^{min} are the upper and lower borders of the search range, respectively.

Step 2. Above two populations are merged and then divided it into two populations with equal number of individuals by random grouping. Fitness of all individuals are calculated to obtain the current global optimal solution *PBest*. The optimal solutions *AgBest* and *BgBest* of pigeon groups A and B are compared, the one with smaller fitness is selected as the current global optimal solution *PBest*.

Step 3. Enter the map and compass operator navigation stage. The maximum iteration number of the map and compass operator is set to K_1. Updating the positions of individuals based on *PBest* and quantum wave function $\ln(1/\varphi)$:

$$P_i^j(k+1) = \begin{cases} R + \tau \cdot |P_{mbest}^j(k) - P_i^j(k)| \cdot \ln(1/\varphi), \varphi > 0.3 \\ R - \tau \cdot |P_{mbest}^j(k) - P_i^j(k)| \cdot \ln(1/\varphi), \varphi \leq 0.3 \end{cases} \quad (i=1,2,\cdots,M; k=1,2,\cdots,K_1; j=1,2) \tag{9}$$

$$\tau = \frac{0.5 \cdot (k - K_1)}{K_1} + 0.5$$
$$R = \frac{\eta_1 \cdot P_i^{j-pbest}(k) + \eta_2 \cdot PBest}{\eta_1 + \eta_2} \tag{10}$$

$$P_i^{j-Lnew}(k) = P_i^j(k) + \gamma \cdot [PBest - \ell \cdot P_{mbest}^j(k)] \quad (i=1,2,\cdots,M_k; \ k=K_1+1,\cdots,K_1+K_2; j=1,2)$$
$$\ell = round(1 + \varpi) \tag{15}$$

Where k is the current number of iteration. $\varphi \in (0,1)$, η_1, $\eta_2 \in rand(0,1)$. The average value of position vector of all individuals in the j-th pigeon group is noted as P_{mbest}^j. The $P_i^{j-pbest}$ stands for the local optimal position of i-th individual in the j-th pigeon group.

Step 4. Compute the fitness of new individuals and update the local optimal solution. The individual with the smallest fitness is retained as

the local optimal solution. Then, the local optimal solution is chaotic mapped to generate the new individuals P_i^{j-Cnew}. The fitness of the new individuals are calculated and the local optimal solution is updated.

$$P_i^{j-Cnew}(k) = (PBest + G_j(i+1)) / 2 \tag{11}$$

Finally, *AgBest* and *BgBest* are compared, and the one with smaller fitness is reserved as the local optimal solution *PBest* of this iteration.

Step 5. Judge whether the current iteration has reached the maximum iteration number of the map and compass operator. If so, the *PBest* is regarded as the current global optimal solution *gBest*, then continue to next step. Otherwise, return to step 3.

Step 6. Enter the landmark operator navigation stage. The maximum iteration number of landmark operator is set as K_2. Individuals are arranged from small to large based on their fitnesses. Then, according to the elite retention strategy, the individuals with small fitness in the first half of the population are retained, and the second half was abandoned according to the elite retention strategy. Both the number of retained individuals in two populations are:

$$M_k = \begin{cases} M_k/2, M_k = 2i \\ (M_k+1)/2, M_k = 2i-1 \end{cases} \quad (i=1,2,\cdots,M) \tag{12}$$

Where $k \in [K_1+1, K_{1+} K_2]$, M_k is the population size of current pigeon groups and its initial value is M.

Step 7. The location of landmark is calculated by Eq. (13), and the retained individuals are guided to the nest:

$$P_{center}^j(k) = \frac{\sum_{i=1}^{M_k} P_i^j(k) \cdot J[P_i^j(k)]}{M_k \sum_{i=1}^{M_k} J[P_i^j(k)]} \quad (k=K_1+1,\cdots,K_1+K_2; j=1,2) \tag{13}$$

$$P_i^j(k+1) = P_i^j(k) + \theta \cdot [P_{center}^j(k) - P_i^j(k)] \quad (i=1,2,\cdots,M_k; j=1,2) \tag{14}$$

Where $\theta \in (0, 1)$, P_{centre}^j stands for the center of j-th pigeon group.

Step 8. The learning factor ℓ is introduced to guide the individuals approach to the optimal solution. Then, make greedy choice between the new position vectors and originals according to their fitness values.

$$P_i^j(k+1) = \begin{cases} P_i^{j-Lnew}(k), J[P_i^{j-Lnew}(k)] < J[P_i^j(k)] \\ P_i^j(k), J[P_i^{j-Lnew}(k)] \geq J[P_i^j(k)] \end{cases} \tag{16}$$

Where $P_i^{j-Lnew}(k)$ is the new position vector of k-th iteration. γ, $\varpi \in (0, 1)$.

Step 9. Calculate the fitness of the updated individuals and update the

AgBest and *BgBest*. Finally, the global optimal solutions *AgBest* and *BgBest* of populations A and B are compared, the one with the smaller fitness is regarded as the global optimal solution *PBest* in current iteration.

Step 10. Judge whether the current iteration number has reached the maximum iteration number of the landmark operator stage. If so, the *PBest* is regarded as the global optimal solution *gBest* of the whole optimization process. Then, the *gBest* is returned to the EADRC framework as optimal parameters matrix. Otherwise, return to step 6.

Correspondingly, the two-stage optimization, parallel search of bi-quantum population, elite retention strategy based on the halving pigeon population and the elite learning mechanism make the BQPIO achieve the accurate and fast optimization performance. The Pseudo code of the BQPIO algorithm is exhibited in Algorithm 1.

Algorithm 1. BQPIO

Start.

Initializations of population size M, search dimension D_P, map and compass operator maximum iteration number K_1, landmark operator maximum iteration number K_2, search range $[P^{min}, P^{max}]$, pigeon populations A and B, local optimal solution **AgBest** and **BgBest** in populations A and B, current global optimal solution PBest.

While $(k \leq K_1)$

For j = 1: 2

For i = 1: M

Update $P_i^j(k+1)$ by Eq. (9).

if $P_i^j(k+1) > P^{max}$

Update $P_i^j(k+1)$ by Eq. (8).

end

if $P_i^j(k+1) < P^{min}$

Update $P_i^j(k+1)$ by Eq. (8).

end

end

end.

Fitness calculation and update $P_i^{j-pbest}(k)$ and P_{mbest}^j, fitness calculation of the new individual P_i^{j-Cnew} generated in chaotic mapping via Eq. (11), obtain the current global optimal solution **PBest**.

end while.

While $(K_1 + 1 \leq k \leq K_2)$

Pigeons are sorted from small to large according to their fitness and the individuals with lower fitness are retained. The number of retained pigeons $\mathbf{M_k}$ is computed by Eq. (12). Then, calculating the landmark location $P_{center}^j(k)$ of pigeons via Eq. (13).

For j = 1: 2

For i = 1:M.

Update $P_i^j(k+1)$ by Eq. (14).

if $P_i^j(k+1) > P^{max}$

Update $P_i^j(k+1)$ by Eq. (8).

end

if $P_i^j(k+1) < P^{min}$

Update $P_i^j(k+1)$ by Eq. (8).

end.

Obtain new position $P_i^{j-Lnew}(k)$ of individuals by Eq. (15).Then, update $P_i^j(k+1)$ via making greedy choice by Eq. (16).

end

end.

Update $P_i^{j-pbest}(k)$, P_{mbest}^j, **AgBest**, **BgBest** and **gBest**.

end while

return global optimal solution **gBest**

end.

4. Simulations and experimental evaluations

To verify the flexible operation capacity of the USC unit regulated by the EADRC strategy, simulations are carried out in the following step. Firstly, the search accuracy and convergence speed of the BQPIO algorithm are tested on the CEC2014 test library. Secondly, the optimal parameters of EADRC scheme are obtained by the validated BQPIO algorithm. the USC unit is guided to meet the flexibility requirements via minimizing the multi-objective function. Then, to confirm the superiority of EADRC, control performance of USC unit respectively regulated by three industrial control strategies (EADRC + BQPIO, ADRC + BQPIO, PID + BQPIO) are given out. All simulations are carried out based on the on-site data of a 1000 MW USC unit in northern China. The experimental platforms are MATLAB 2021a and SIMULINK 2021a on a PC with AMD Ryzen 5 3500 × 3.6G CPU and 8 GB RAM.

4.1. Performance verification of BQPIO based on benchmark functions

4.1.1. Selections of benchmark functions and comparison algorithms

In the EADRC designing, the parameters choices play a key role to its control performance. However, the parameters of EADRC are usually tuned by manual in engineering which is tedious and time-consuming. On the contrary, the heuristic method has simple principle and strong scalability which reveal excellent superiority in parameters optimization. Thus, considering the prominent optimization capacity of PIO, the BQPIO algorithm as a promotion of conventional PIO is presented. Before using the BQPIO algorithm to obtain the optimal parameters of EADRC scheme, a performance test of BQPIO is required.

The CEC 2014 [57] is regarded as the benchmark functions library to provide a desired platform for the presented BQPIO performance test. There are 30 functions of four typical categories totally included in CEC 2014, namely unimodal function, simple multimodal function, hybrid function and composition function. Considering the similarity among the functions in the same category and test complexity, 12 benchmark functions include 3 unimodal functions, 3 simple multimodal functions, 3 hybrid functions and 3 composition functions are selected to carry out the performance tests. The selected test functions are listed in Table 1. Since the development maturity and effectiveness of a certain optimization algorithm are main factors considered in comparison test designing, the PIO, PSO, artificial bee colony (ABC) and emperor penguin optimization (EPO) algorithms are chosen as contrast algorithms here. The PSO, ABC and EPO algorithms are selected for comparison from their representative significance in the field of heuristic algorithms. For decreasing the occasionality of results, 50 executed are repeated for each test and the optimal one is selected. All the 3000 (12 × 5 × 50) tests in total are carried out in the same experimental environment to achieve a fair comparison. In Table 1, F_i^* stands for the optimal solution of

Table 1
The selected 12 benchmark functions from CEC 2014 for the performance tests of CBQPIO algorithm.

Categories	Functions	F_i^*	Range
Unimodal functions	F_1 Rotated High Conditioned Elliptic Function	100	$[-100,100]^D$
	F_2 Rotated Bent Cigar Function	200	$[-100,100]^D$
	F_3 Rotated Discus Function	300	$[-100,100]^D$
Simple Multimodal Functions	F_6 Shifted and Rotated Weierstrass Function	600	$[-100,100]^D$
	F_{10} Shifted Schwefel's Function	1000	$[-100,100]^D$
	F_{16} Shifted and Rotated Expanded Scaffer's F6 Function	1600	$[-100,100]^D$
Hybrid functions	F_{17} Hybrid Function 1 ($N = 3$)	1700	$[-100,100]^D$
	F_{20} Hybrid Function 4 ($N = 4$)	2000	$[-100,100]^D$
	F_{22} Hybrid Function 6 ($N = 5$)	2200	$[-100,100]^D$
Composition functions	F_{23} Composition Function 1 ($N = 5$)	2300	$[-100,100]^D$
	F_{25} Composition Function 3 ($N = 3$)	2500	$[-100,100]^D$
	F_{29} Composition Function 7 ($N = 3$)	2900	$[-100,100]^D$

Table 2
Parameters setting of five optimization algorithms in the performance tests.

Parameters	BQPIO	PIO	PSO	ABC	EPO
M	100	100	100	100	100
D	30	30	30	30	30
K_1 (map and compass operator)	$50D$	$50D$	/	$50D$	/
K_2 (landmark operator)	$50D$	$50D$	/	$50D$	/
K (Maximum number of iterations)	$100D$ $(50D + 50D)$	$100D$ $(50D + 50D)$	$100D$	$100D$	$100D$
ω (Inertia weight)	/	/	0.5	/	/
c_1, c_2 (Acceleration constant)	/	/	1.4	/	/
C_O (Compass factor)	/	/	/	/	0.7
Q (Motion parameters)	/	/	/	/	2
l_1, l_2 (exploitation factors)	/	/	/	/	2
$Limit$ (Maximum for honey stay)	/	/	/	10	/
s (Earch number)	/	/	/	5	/

Table 3
Statistic results of performance indicators in benchmark functions optimization tests using different algorithms.

Categories	Functions	Indicator	BQPIO	PIO	ABC	PSO	EPO
Unimodal functions	F1	Best	1.102E+02	4.228E+04	3.758E+05	1.608E+02	5.743E+05
		Mean	**1.337E + 05**	6.652E+05	1.490E+07	5.670E+05	4.763E+08
		SD	**3.066E + 05**	3.850E+05	1.182E+07	2.213E+06	2.702E+08
		T_C	**1.970s**	2.440s	5.820s	9.060s	12.540s
	F_2	Best	11.529E+03	**3.172 E + 02**	6.454E+09	1.489E+10	3.091E+09
		Mean	**2.511E + 03**	3.875E+03	7.869E+09	3.486E+10	8.086E+09
		SD	**3.114E + 03**	3.776E+03	4.758E+08	1.426E+10	2.008E+09
		T_C	**1.840s**	3.290s	5.980s	8.740s	10.720s
	F_3	Best	**3.020E-01**	5.900E-01	9.272E+03	1.067E+04	1.110E+05
		Mean	**3.560E + 03**	6.811E+03	1.321E+04	1.936E+04	9.815E+05
		SD	**1.843E + 03**	6.220E+03	1.416E+04	4.102E+03	1.336E+06
		T_C	**1.130s**	1.859s	6.240s	8.810s	15.060s
Simple Multimodal Functions	F_6	Best	**4.160E-01**	6.659 E+00	9.479E+00	1.033E+01	1.305E+00
		Mean	**4.311E + 00**	1.061E+01	1.539E+01	2.271E+01	9.849E+00
		SD	**2.107E-01**	1.138 E+00	3.930 E−01	9.820E-01	3.280E+00
		T_C	**2.600s**	5.130s	7.510s	18.200s	14.010s
	F_{10}	Best	**2.210E + 01**	1.069E+03	1.138E+03	1.967E+03	2.842E+01
		Mean	**8.299E + 02**	1.834E+03	1.735E+03	2.488E+03	9.009E+02
		SD	3.663E+02	3.708E+02	2.101E+02	**1.819E + 02**	3.767 + 02
		T_C	**3.440s**	5.870s	3.862s	9.641s	18.120s
	F_{16}	Best	**1.477E + 00**	3.664E+00	3.881E+00	3.573E+00	2.213E+00
		Mean	**3.096E + 00**	7.138E+00	4.542E+00	3.957E+00	5.297E+00
		SD	1.200E-01	2.250E-01	**1.510E-01**	5.240E-01	4.710E-01
		T_C	**1.950s**	2.400s	5.320s	8.995s	12.750s
Hybrid functions	F_{17}	Best	**2.049E + 02**	2.186E+05	2.894E+05	4.678E+05	2.302E+02
		Mean	**6.899E + 03**	7.604E+05	4.087E+05	2.279E+07	8.833E+03
		SD	**1.587E + 04**	3.314E+05	6.732E+04	1.957E+07	1.706E+04
		T_C	**2.020s**	4.600s	14.770s	9.350s	25.610s
	F_{20}	Best	**3.134E + 01**	4.066E+03	3.994E+03	6.125E+05	5.737E+01
		Mean	**1.652E + 03**	2.399E+04	1.036E+04	2.096E+07	1.959E+04
		SD	**5.530E + 03**	1.972E+04	6.002E+03	2.403E+07	5.688E+04
		T_C	**2.600s**	5.580s	5.410s	9.120s	14.000s
	F_{22}	Best	**2.195E + 01**	1.877E+02	3.680E+02	5.133E+02	3.072E+01
		Mean	**1.229E + 02**	6.204E+02	4.908E+02	8.517E+02	1.511E+02
		SD	1.009E+02	1.397E+02	**4.861E + 01**	1.202E+02	1.667E+02
		T_C	1.330s	**0.900s**	6.000s	9.500s	19.120s
Composition functions	F_{23}	Best	**2.000E-02**	2.015E+02	2.095E+02	6.069E+02	3.294E+02
		Mean	**2.097E + 02**	4.220E+02	3.034E+02	1.053E+03	3.867E+02
		SD	**3.869E + 00**	6.121E+01	7.949E+01	2.986E+02	1.370E+01
		T_C	**1.170s**	2.290s	8.200s	12.040s	11.460s
	F_{25}	Best	**1.261E + 02**	1.996E+02	1.683E+02	2.000 E+02	1.373E+02
		Mean	**1.932E + 02**	4.031E+02	2.702E+02	2.386E+02	2.129E+02
		SD	**1.240E-01**	6.380 E−01	1.841E+01	2.245E+01	2.004E+01
		T_C	**3.200s**	4.180s	7.960s	17.400s	27.870s
	F_{29}	Best	**3.525E + 02**	8.617E+03	3.906E+06	1.752E+06	3.955E+02
		Mean	**6.099E + 04**	3.416E+05	1.344E+08	8.142E+06	5.683E+05
		SD	**5.920E + 04**	9.993E+05	7.115E+07	4.668E+06	1.584E+06
		T_C	**1.300s**	6.090s	9.520s	13.160s	19.430s

corresponding function in search range [−100,100] under D dimension.

4.1.2. Parameters determination of comparison algorithms

The dimension of the benchmark function is set to $D = 30$ for verifying the effectiveness of BQPIO algorithm in dealing with high-dimensional problems. Except for the unique parameters of each algorithm, all the common parameters are equally set and shown in Table 2.

4.1.3. Benchmark functions test results

Performance tests are carried out based on the 12 benchmark functions and 5 contrast algorithms. Four statistic indicators including the minimum value (*Best*), mean value (*Mean*) and standard deviation (*SD*) of optimization error and total computing time (*Time*) are displayed in Table 3 for proving the superiorities of BQPIO. The definitions of Mean and SD are shown in Eq. 17 and 18.

$$Mean = \frac{1}{N_{re}} \sum_{i=1}^{N_{re}} F^i \tag{17}$$

$$SD = \sqrt{\frac{1}{N_{re}} \sum_{i=1}^{N_{re}} \left(F^i - Mean \right)^2} \tag{18}$$

Where N_{re} is the repeated time of each test and its value is set to 50 here. The optimization value of corresponding function in the i-th test is noted as F^i.

As presented in Table 3, the proposed BQPIO reveals overwhelming advantages in the optimization of F_1, F_3, F_6, F_{16}, F_{17}, F_{20}, F_{23}, F_{25} and F_{29}. Although some other algorithms exhibit higher optimization accuracy of F_2, F_{10} and F_{22}, the computing speed of BQPIO is prominent in most cases. Therefore, the BQPIO is proved to be a successful attempt simultaneously considering exploration and exploitation.

4.2. EADRC optimized by BQPIO

Adding the information of unit is conducive to reduce the estimation burden of ESO for control performance improvement. Therefore, the state space model of SUC unit given in Eq. (19) is obtained by the subspace identification method [58] based on its 5000 sets on-site data at first. The operating conditions of USC unit under various rated load are

also displayed in Table 4. Then, the BQPIO algorithm with excellent exploration ability is used to automatically attain the optimal parameters of EADRC strategy to improve the operational flexibility of USC unit.

For fair comparisons, parameters in ADRC and PID methods are also optimized by the BQPIO algorithm. In all the parameters optimization processes, the parameter settings of BQPIO algorithm are remained unchanged expect for individual dimension D_P. The individual dimension D_P is determined by the number of parameters to be tuned in controller. Considering the rationality and experience in the designing of EADRC scheme, the parameters search range is set as $[0.05, 50]^{D_P}$. There are totally 9 parameters in EADRC strategy to be undetermined, then D_P is equal to 9. The maximum iteration number of compass operator K_1 and landmark operator K_2 are respectively set to 20 and 30. And the population size M, constant factors φ, θ, γ and ϖ are set as 30, 0.7,0.4,0.22 and 0.19, respectively. As a rule of thumb, the weight factors w_1 and w_2 are assigning as 0.7 and 0.3, respectively. The parameters optimization of EADRC shown in Algorithm 1 is taken as example, other control methods are similar. Parameters optimization results of all control methods are displayed in Table 5. Particularly, P_s and I_s ($s=$ 1,2,3) are the proportional and integral coefficients of decoupling PID controllers. b_{0A} and ω_{cA} are the optimal parameters in ADRC control strategy.

4.3. Tracking performance test

In the setpoint tracking performance test, the load ramping rate and shedding rate are respectively set to 3.3% MCR/min and 5.5% MCR/min. Simulations are carried out to test the flexible operation ability of USC unit within the wide-load ranges of [30% RBL, 90% RBL]. In the tests, the USC unit can experience the deep peak shaving and normal load regulation processes. The amplitude of each load variation is set as 100 MW. Responses of output variables and manipulated variables of USC are illustrated in Figs. 4–5. For standardly evaluating the load tracking performance of USC unit regulated by different control methods, the total objective function value J, settling time t_s and smoothness of manipulated variables (shown in Eq. (20)) are chosen as evaluation indicators. The performance indicators for unit to response to the load demands are recorded in Table 6.

Table 4
The operating conditions and model of 1000 MW USC unit under various rated load.

$$\dot{x}(k+1) = A^m x(k) + B^m u(k)$$
$$y(k) = C^m x(k) + D^m u(k)$$
$$u = \begin{bmatrix} u_B & \mu_T & u_W \end{bmatrix}; y = \begin{bmatrix} N & P_T & T \end{bmatrix}$$

$$A^m = \begin{bmatrix} -10.92 & 6.86 & -2.26 & -6.19 \\ 15.44 & -10.09 & 6.14 & 3.07 \\ 19.47 & -37.58 & -13.48 & -14.60 \\ 30.82 & -53.10 & -14.48 & -29.05 \end{bmatrix}; B^m = \begin{bmatrix} -0.35 & -0.02 & 0.03 \\ 0.24 & 0.02 & 0.07 \\ -1.90 & 0.03 & 0.06 \\ -3.08 & 0.11 & 0.09 \end{bmatrix}; C^m = \begin{bmatrix} -358.10 & 171.50 & -94.62 & 2.80 \\ -13.36 & 0.03 & 0.03 & 0.05 \\ -275.8 & -180.80 & -9.80 & 0.38 \end{bmatrix}; D^m = 0 \tag{19}$$

Operating condition	N(MW)	P_T (MPa)	T(°C)	μ_T (%)	u_B (t/h)	u_W (t/h)
90% rated load	917.55	24.07	381.47	88.06	318.38	2147.09
80% rated load	816.97	21.80	376.00	85.37	279.75	1976.60
70% rated load	715.22	19.91	370.90	84.60	242.39	1798.11
60% rated load	617.05	18.04	366.10	81.52	205.10	1615.62
50% rated load	517.07	15.80	361.94	79.03	167.80	1435.00

Table 5
Parameter optimization results of different control strategies based on the BQPIO algorithm.

Control strategies	Parameters		
EADRC + BQPIO	$b_{01} = 28.111$ $\omega_{o1} = 9.200$ $\omega_{c1} = 4.583$	$b_{02} = 10.400$ $\omega_{o2} = 20.150$ $\omega_{c2} = 5.864$	$b_{03} = 0.126$ $\omega_{o3} = 22.377$ $\omega_{c3} = 5.993$
ADRC + BQPIO	$b_{0A1} = 24.216$ $\omega_{cA1} = 3.829$	$b_{0A2} = 5.050$ $\omega_{cA2} = 8.264$	$b_{0A3} = 0.600$ $\omega_{cA3} = 1.300$
PID + BQPIO	$P_1 = 3.700$ $I_1 = 0.800$	$P_2 = 19.180$ $I_2 = 18.020$	$P_3 = 14.359$ $I_3 = 6.400$

$$TV_s = \int_0^{T_{max}} (u_s(t+1) - u_s(t))dt, s = 1, 2, 3 \quad (20)$$

As exhibited in Fig. 4, lines with different colors and line-type stand for the load regulation effect of USC unit combined with diverse control techniques. The variations of output power, main steam pressure and intermediate point temperature in USC unit are respectively drawn in Fig. 4(a), (b) and (c) under various load demands. Thanks to the EADRC + BQPIO algorithm, USC unit can quickly change its output power to suppress the randomness of renewable energy sources. During the deep peak shaving process (0s–880s), the load demand reveals the fastest load shedding rate and highest tracking accuracy by USC unit based on the EADRC + BQPIO algorithm, then is the ADRC + BQPIO method. As shown in Fig. 4(a), when USC unit is regulated by the EADRC + BQPIO strategy represented by the red solid line, its output power curve is very close to the setpoint value. And the main steam pressure and temperature of USC unit are fluctuating within the smallest ranges according to Fig. 4(b ~ c). It can be seen from Table 6 that the load tracking error e_s of USC unit regulated by EADRC + BQPIO strategy are only 0.3547 MW and 1.942 MW while the ADRC + BQPIO strategy are 2.236 MW and 4.460 MW. The settling times t_s of USC unit combined the EADRC + BQPIO scheme are respectively reduced to 137.8s and 123.2s from

272.2s to 260.5s compared to the PID + BQPIO method. Then, the percentage improvements of the EADRC + BQPIO strategy versus the ADRC + BQPIQ in tracking errors are 75.53% and 56.45% while they are 20.57% and 21.73% in settling times according to Table 7. Thereby, the flexible operation capacity of USC unit is promoted thanks to the EADRC + BQPIO scheme. As to the operational economy J, the percentage improvements for EADRC + BQPIO based USC unit versus the ADRC + BQPIQ algorithm are 21.44% and 22.48%. Furthermore, as can be seen from Fig. 5(a), the position of main steam valve in USC unit based on the EADRC + BQPIO is remained relatively stable that is favor to extend its service life. Regulated by the EADRC + BQPIO technology with remarkable control performance, the load demands can be reached by the minimum variations of coal feeding rate and water feeding rate of unit. Hence, the smoothness of manipulated variables of USC unit regulated by the EADRC + BQPIO strategy are fully verified by the least values of TV_1, TV_2 and TV_3. The suitable water-coal-ratio reveals the most prominent safe operation ability of boiler. It is also can be seen from Table 8 that the settling time for the three output variables in USC unit are respectively reduced to 172.950s, 232.875s and 186.375s due to the EADRC + BQPIO algorithm. Benefit from the integrated EADRC + BQPIO strategy, the mean load tracking error for USC to response to load requirements is 3.052 MW which is 65.37% of the ADRC + BQPIO method. Thus, transforming the USC unit by EADRC + BQPIO strategy, the improved deep peak shaving ability is attained which is advantageous to its flexible operation.

As shown in Fig. 4, combined with the superior EADRC + BQPIO scheme, the USC unit can also obtain the most remarkable load ramping rate and tracking accuracy during the load rising process(880s–4000s). As recorded in Table 7, except for the load changes of 317 MW–417 MW, the load tracking error of the USC unit based on the EADRC + BQPIO algorithm are 9.74%, 70.72%, 37.50%, 22.33% and 46.31% of ADRC + BQPIQ. Compared to the ADRC + BQPIO algorithm, the settling times for USC unit which regulated by the EADRC + BQPIO strategy to response to load demands are all reduced by more than 6%. Especially,

Table 6
The performance comparison of USC unit under different controllers in the tracking performance test.

| Time (s)	Load changes	Controller	e_s (MW)	t_s (s)	TV_1	TV_2	TV_3	J
$t = 0s$–440s	517 MW–417 MW	EADRC + BQPIO	**0.547**	**137.800**	**106.960**	**310.099**	**713.232**	**5472.806**
		ADRC + BQPIO	2.236	173.500	605.451	475.824	788.300	6966.142
		PID + BQPIO	2.613	272.200	722.230	480.594	801.285	7107.935
$t = 440s$–880s	417 MW–317 MW	EADRC + BQPIO	**1.942**	**123.200**	**759.445**	**323.431**	**16589.223**	**6034.684**
		ADRC + BQPIO	4.460	157.400	1478.969	519.124	22193.536	7784.886
		PID + BQPIO	4.694	260.500	2037.941	541.201	22995.297	10531.589
$t = 880s$–1320s	317 MW–417 MW	EADRC + BQPIO	1.998	**184.800**	1232.195	508.614	25266.300	10253.504
		ADRC + BQPIO	**0.290**	197.500	**1220.432**	**503.600**	**25016.177**	**10159.416**
		PID + BQPIO	0.578	212.700	3356.476	925.156	47881.252	17873.850
$t = 1320s$–1760s	417 MW–517 MW	EADRC + BQPIO	**7.644**	**199.000**	**1450.415**	**596.640**	**29512.093**	**12167.733**
		ADRC + BQPIO	8.469	215.800	1461.592	901.273	29742.771	12260.084
		PID + BQPIO	8.651	297.800	3988.762	997.421	30693.176	21342.227
$t = 1760s$–2200s	517 MW–617 MW	EADRC + BQPIO	**1.395**	**186.800**	**1806.072**	**803.486**	**40020.597**	**15913.832**
		ADRC + BQPIO	4.764	216.500	2009.514	824.892	40689.488	16943.210
		PID + BQPIO	4.955	298.400	3490.446	1180.812	57852.838	21467.858
$t = 2200s$–2640s	617 MW–717 MW	EADRC + BQPIO	**2.795**	**184.700**	**2145.190**	**879.241**	**43283.416**	**18151.922**
		ADRC + BQPIO	4.472	214.200	2411.392	988.240	48642.281	20409.629
		PID + BQPIO	4.668	300.700	3956.913	1810.483	53334.639	35472.358
$t = 2640s$–3080s	717 MW–817 MW	EADRC + BQPIO	**4.195**	**183.000**	**2441.119**	**999.310**	**49114.373**	**20125.080**
		ADRC + BQPIO	5.401	211.100	2504.197	1025.093	50379.035	22714.942
		PID + BQPIO	5.634	299.600	4168.572	1880.091	56969.849	36920.224
$t = 4000s$–3520s	817 MW–917 MW	EADRC + BQPIO	**3.896**	**184.300**	**2725.000**	**1114.457**	**54703.462**	**23175.422**
		ADRC + BQPIO	7.256	215.000	2798.804	1144.608	56181.301	23804.680
		PID + BQPIO	7.249	302.000	4759.018	2045.796	8358.730	40248.208
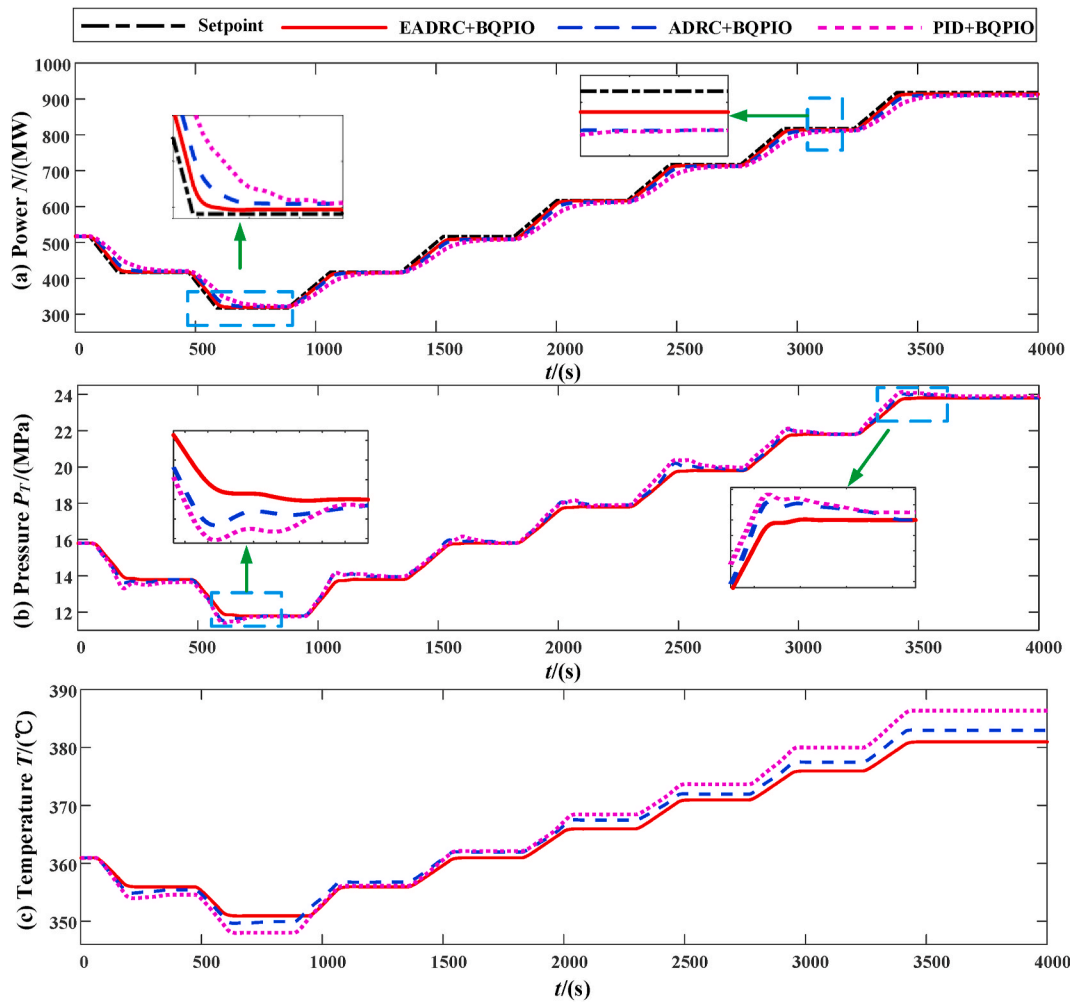
Fig. 4. Responses of output variables in USC unit with the load setpoint variations under wide-load ranges from 30%RBL to 90% RBL.

Table 7

The percentage improvement of the EADRC + BQPIO versus the next ADRC + BQPIQ in the tracking performance test and disturbances rejection ability test.

| Test	Time (s)	Changes	Controller	Improvement (%)						
				e_s	t_s	σ	TV_1	TV_2	TV_3	J
Tracking performance test	$t = 0s$–440s	517 MW–417 MW	EADRC + BQPIO	75.53	20.57	/	82.33	34.83	9.52	21.44
	$t = 440s$–880s	417 MW–317 MW	EADRC + BQPIO	56.45	21.73	/	48.65	37.70	25.30	22.48
	$t = 880s$–1320s	317 MW–417 MW	EADRC + BQPIO	−588.96	6.43	/	−0.96	−0.99	−1.00	−0.92
	$t = 1320s$–1760s	417 MW–517 MW	EADRC + BQPIO	9.74	7.78	/	0.76	33.80	0.78	0.75
	$t = 1760s$–2200s	517 MW–617 MW	EADRC + BQPIO	70.72	13.71	/	10.12	2.60	1.64	6.08
	$t = 2200s$–2640s	617 MW–717 MW	EADRC + BQPIO	37.50	13.77	/	11.04	11.02	11.01	11.06
	$t = 2640s$–3080s	717 MW–817 MW	EADRC + BQPIO	22.33	13.30	/	2.52	2.51	2.51	11.40
	$t = 3080s$–4000s	817 MW–917 MW	EADRC + BQPIO	46.31	14.27	/	2.64	2.63	2.63	2.64
Disturbances rejection ability test	$t = 120s$	Active power (+20 MW)	EADRC + BQPIO	/	45.63	84.41	69.51	59.43	40.33	41.36
	$t = 480s$	Main steam pressure (+0.2 MPa)	EADRC + BQPIO	/	13.70	41.53	3.26	3.08	2.70	−3.23
	$t = 840s$	Intermediate point temperature (+10 °C)	EADRC + BQPIO	/	−19.62	1.15	0.28	0.89	3.27	3.09
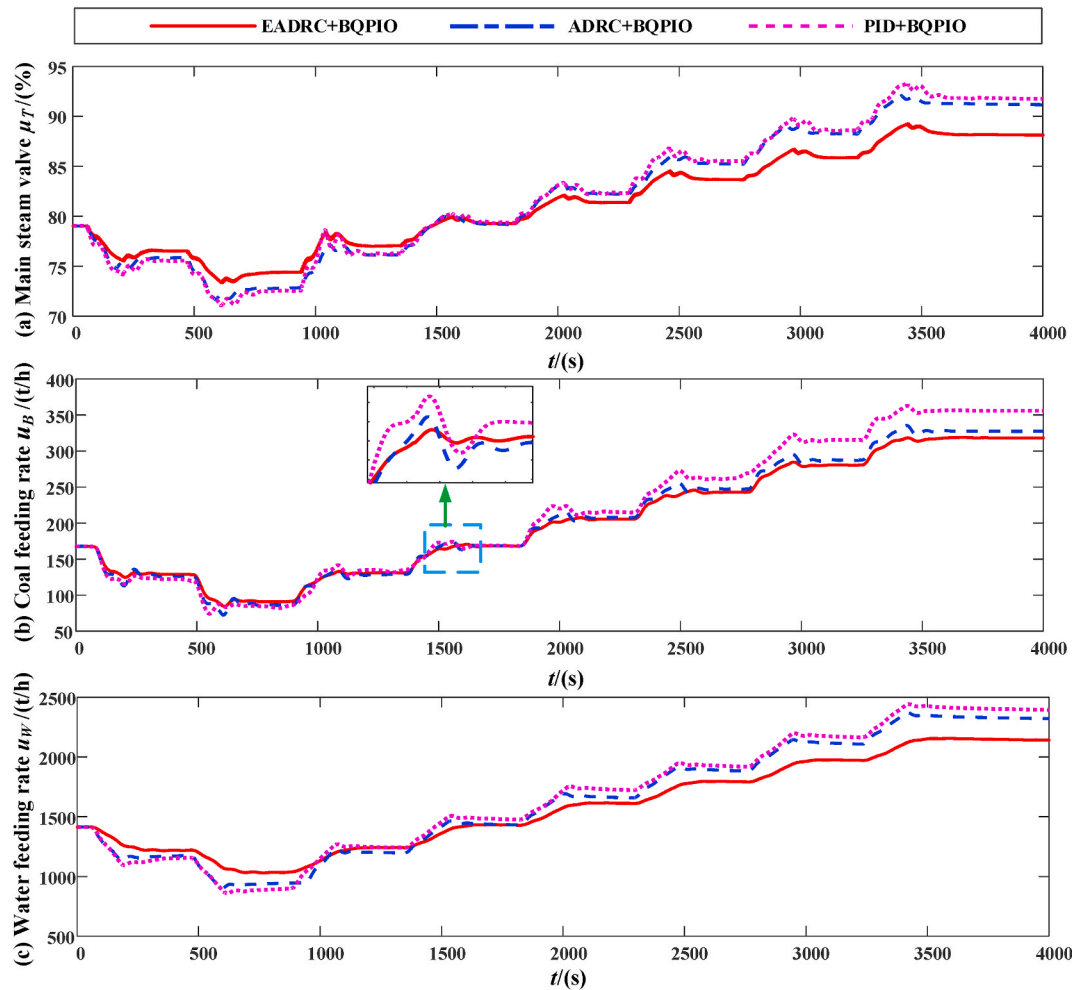
Fig. 5. Responses of manipulated variables in USC unit with the load setpoint variations under wide-load ranges from 30%RBL to 90% RBL.

Table 8
The improvement of the EADRC + BQPIO than ADRC + BQPIQ across the entire range from 0 to 4000 s for all three output variables.

Output channel	Controller	Regulation error/Fluctuation range		Regulation time (s)	
		Range	Mean	Range	Mean
Active power e_s (MW)	EADRC + BQPIO	[0.547, 7.644]	3.052	[123.2, 199.0]	172.950
	ADRC + BQPIO	[0.290, 8.469]	4.669	[157.4, 216.5]	200.125
Main steam pressure	EADRC + BQPIO	[1.98, 2.24]	2.048	[203.0, 254.0]	232.875
ΔPt (MPa)	ADRC + BQPIO	[1.90, 2.40]	2.166	[275.0, 451.0]	341.750
Intermediate point temperature	EADRC + BQPIO	[4.85, 5.00]	4.973	[149.0, 213.0]	186.375
ΔT (°C)	ADRC + BQPIO	[4.50, 6.82]	5.609	[181.0, 295.0]	221.375

the main steam pressure and intermediate point temperature of USC unit regulated by the EADRC + BQPIO algorithm fluctuate within the minimum ranges. These desired results effectively avoid the operating accidents caused by excessive temperature and steam pressure of equipments in once-through boiler. Conclusion can be drawn that the capacity of USC unit modified by the EADRC + BQPIO algorithm to rapidly change its output power has been promoted. Moreover, it can be concluded from Fig. 5, the load demands still able be satisfied by USC unit based on the EADRC + BQPIO strategy with the smallest increment of coal feeding rate and water feeding rate. The least TV_1, TV_2, TV_3 noted in Table 6 display the perfect smoothness of manipulated variables of USC unit regulated by the EADRC + BQPIO scheme in all the load response processes. Therefore, the operational economy of unit is promoted due to the remarkable control performance of EADRC + BQPIO. In addition, as depicted in Table 6, except the load range of 317

MW–417 MW, all the load tracking precision of the EADRC + BQPIO based USC unit are the highest. The average load tracking error of USC unit combined with the EADRC + BQPIO method during the load rising process is only 3.653 MW while ADRC + BQPIO and PID + BQPIO algorithms are 5.108 MW and 5.289 MW respectively. What's more, the load demands also reveal the fastest load regulation capacity of USC unit regulated by the EADRC + BQPIO strategy. The average settling time of EADRC + BQPIO method based USC unit during the load rising is reduced to 187.1s while ADRC + BQPIO and PID + BQPIO algorithms are 211.6s and 285.2s respectively. In the entire load regulation process, the load tracking error of USC unit based on the EADRC + BQPIO method is within [0.547 MW, 7.644 MW] when it's [0.290 MW, 8.469 MW] for ADRC + BQPIO algorithm according to Table 8. Benefit from the EADRC + BQPIO strategy, the operation safety of USC unit is effectively improved. At every power variation, the main steam pressure
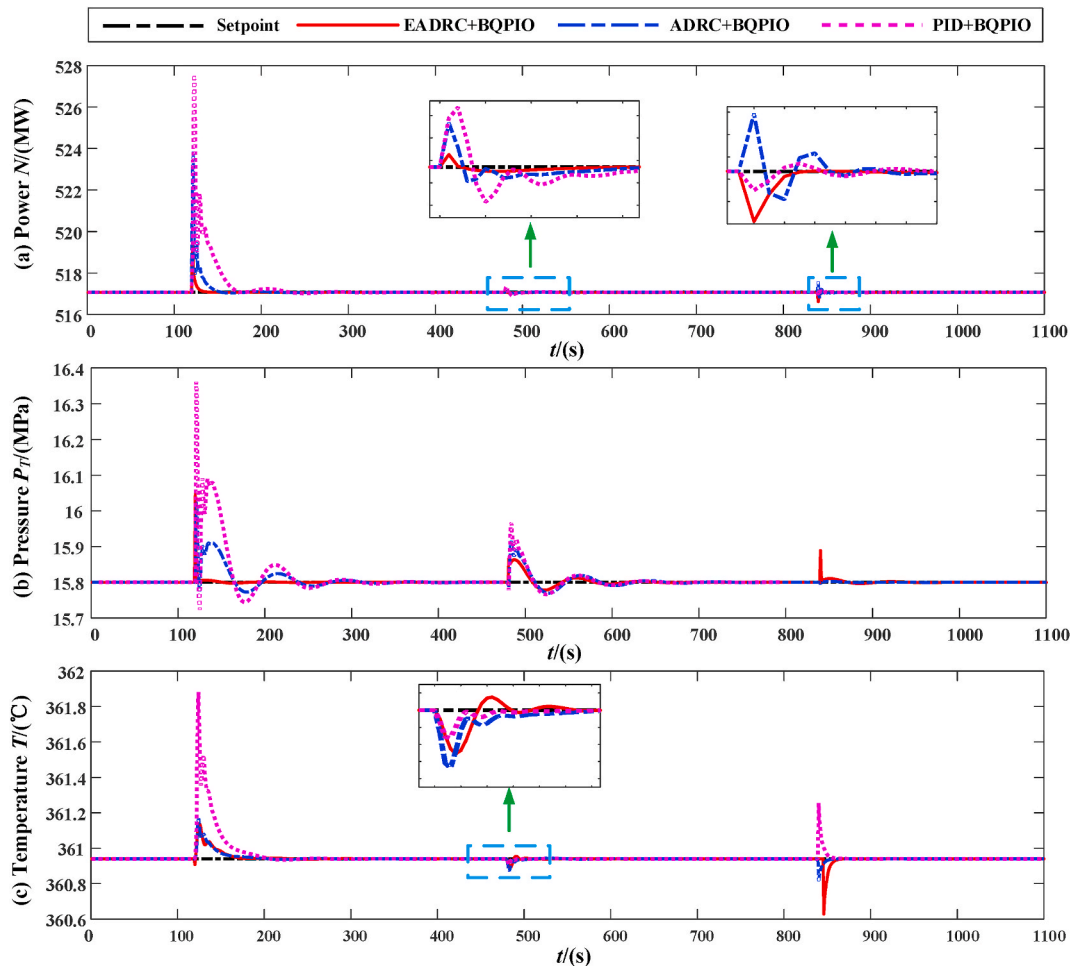
Fig. 6. Responses of output variables of USC unit under 50% rated load with the load, pressure and temperature disturbances additions when $t = 120$s, 480s and 840s, respectively.

Table 9
The performance comparison of USC unit under different controllers in disturbance rejection ability test.

Time (s)	Output variables	Controller	t_s (s)	σ (%)	TV_1	TV_2	TV_3	J
$t = 120$s	Active power (+20 MW)	EADRC + BQPIO	**49.100**	**0.235**	**11.637**	**3.978**	**670.639**	**205.942**
		ADRC + BQPIO	90.300	1.507	38.170	9.806	1123.883	351.182
		PID + BQPIO	126.000	2.030	71.171	17.077	1684.816	531.167
$t = 480$s	Main steam pressure (+0.2 MPa)	EADRC + BQPIO	**148.000**	**0.418**	**89.920**	**19.020**	1136.842	397.049
		ADRC + BQPIO	171.500	0.715	92.954	19.625	1168.440	**384.618**
		PID + BQPIO	201.600	1.044	97.809	20.592	1218.996	401.529
$t = 840$s	Intermediate point temperature (+10 °C)	EADRC + BQPIO	25.000	0.086	68.766	**15.304**	**1182.080**	**379.085**
		ADRC + BQPIO	**20.900**	0.087	68.957	15.441	1221.978	391.154
		PID + BQPIO	27.400	**0.035**	**55.457**	19.080	1502.447	381.008

and intermediate point temperature in EADRC + BQPIO based USC unit fluctuate within [1.98 MPa, 2.24 MPa] and [4.85 °C, 5.00 °C] while they are [1.90 MPa, 2.40 MPa] and [4.50 °C, 6.82 °C] for ADRC + BQPIO. All the three output variables in USC unit achieve improvements thanks to the remarkable control performance of EADRC + BQPIO algorithm. Therefore, employing the EADRC + BQPIO algorithm to USC unit to promote its flexible operation capability under full operating conditions is a successful attempt.

4.4. Disturbance rejection ability test

Disturbances caused by coal quality and load variations in

generation process becomes more and more obvious. Therefore, remarkable disturbance rejection ability is conducive to the flexible operation of USC unit. Then, a positive step disturbance with amplitude of 20, 0.2 and 10 is respectively added into the active power, main steam pressure and intermediate point temperature channels of USC unit when $t = 120$s, 480s and 840s for the disturbance rejection ability tests. Responses of output variables and manipulated variables of USC unit are respectively drawn in Figs. 6 and 7. The disturbance rejection performance indexes of unit based on diverse control methods are recorded in Table 9.

As depicted in Fig. 6, all the disturbances in the output channels of USC unit with the EADRC + BQPIO scheme are fast and accurately
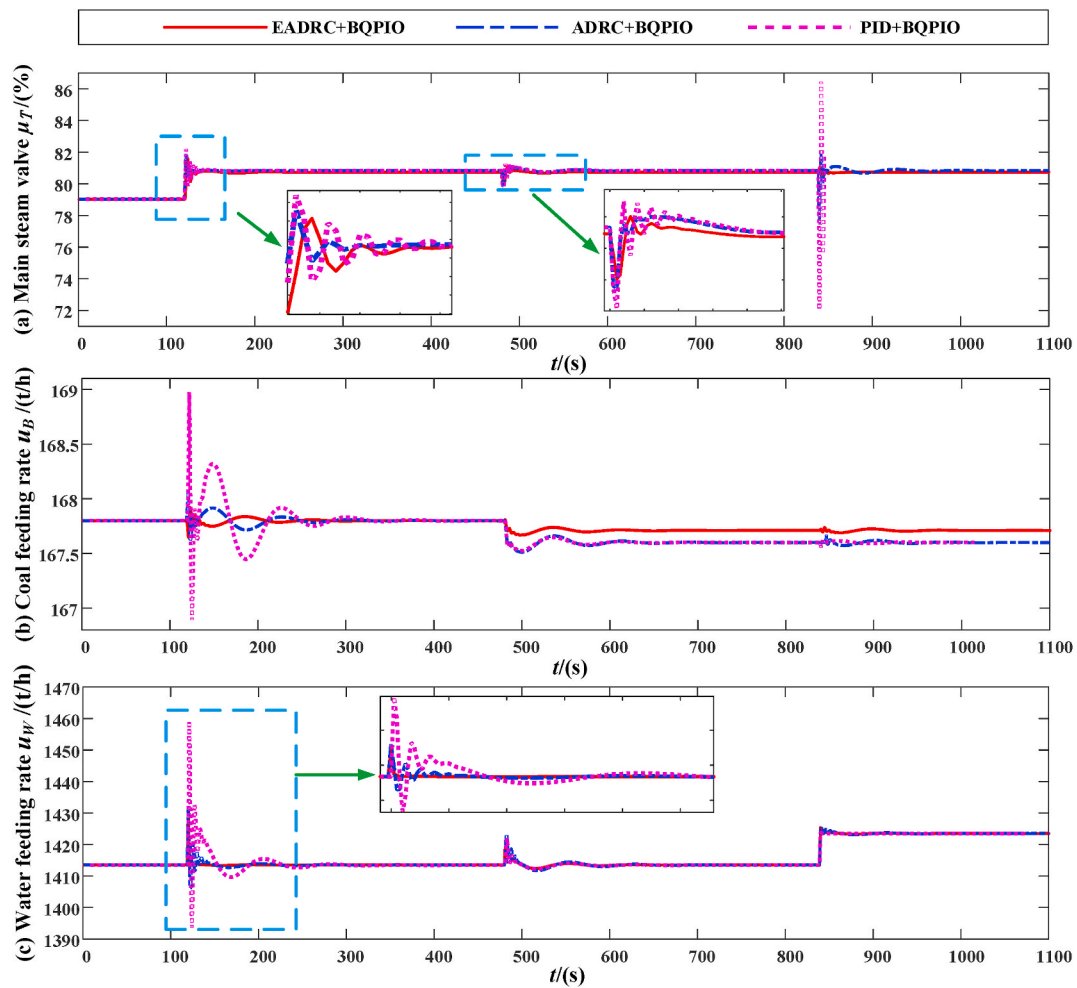
Fig. 7. Responses of manipulated variables of USC unit under 50% rated load with the load, pressure and temperature disturbances additions when $t = 120s$, 480s and 840s, respectively.
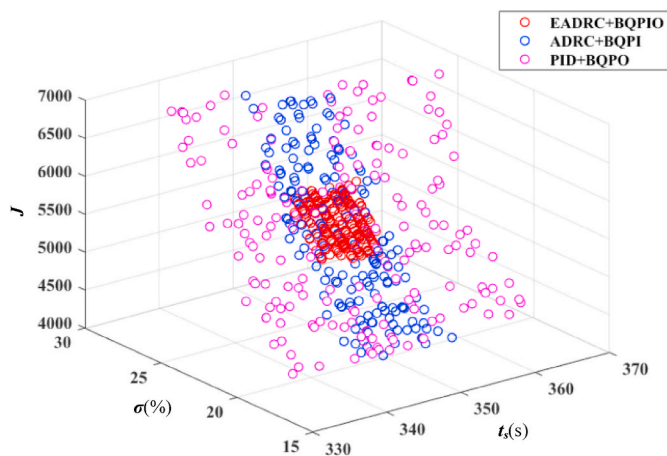

Fig. 8. The scatter distributions of load responses of USC unit when model parameters perturbation and a positive step with the amplitude of 10 are simultaneously added.

suppressed. Meanwhile, the overshoots of the output variables in USC unit are relatively small under the EADRC + BQPIO framework. Besides, as drawn in Fig. 7, all the manipulated variables of USC unit fluctuate in the minimum ranges. According to Table 9, the setting time t_s for EADRC + BQPIO strategy based USC unit to respectively suppress the

disturbance in active power and main steam pressure channels are shortened to 49.1s and 148s while they are 90s and 171.5s by ADRC + BQPIO method. In the suppression process of active power and steam pressure disturbances, the overshoots σ% of USC unit modified by the EADRC + BQPIO scheme are 0.235% and 0.418% while the PID + BQPIO method are 2.03% and 1.044%. The settling time for the active power and main steam pressure channels in the EADRC + BQPIO strategy based unit to reject disturbances are decrease to 45.63% and 13.70% of ADRC + BQPIO according to Table 7. It is shown that the USC unit regulated by the EADRC + BQPIO algorithm has shown an unbeatable position in both the disturbance rejection tests of active power and main steam pressure channels. In the suppression process of temperature disturbance, although the settling time of output variables of USC unit regulated by EADRC + BQPIO is longer than ADRC + BQPIO but the overshoot achieves the improvement of 1.15%. Besides, the smoothness of manipulated variables is satisfactory. Thus, above analysises fully illustrate that the EADRC + BQPIO strategy with invincible disturbance rejection capacity greatly improves the operational flexibility and economy of USC unit under full operating conditions.

4.5. Robustness test

Practically, the operating conditions of unit often change affected by various uncertainties. Therefore, Monte Carlo stochastic tests are carried out to evaluate the robustness of the proposed control approach. Eq. (19) is regarded as the nominal model, its any two parameters (inertia

Table 10
The performance comparison of different controllers in robustness test with 200 samples.

Output channel	Controller	t_s (s)			σ (%)		
		Range	Mean	SD	Range	Mean	SD
Active power	EADRC + BQPIO	**[343.0, 350.0]**	**350.0**	**2.8**	**[19.8, 22.9]**	**21.6**	**1.3**
	ADRC + BQPIO	[339.0, 355.7]	348.2	4.3	[16.7, 27.2]	22.5	2.4
	PID + BQPIO	[333.0, 364.1]	347.0	9.4	[16.4, 25.5]	22.8	2.9
Main steam pressure	EADRC + BQPIO	**[306.5, 314.4]**	**310.3**	**1.2**	**[6.9, 16.1]**	**10.4**	**1.1**
	ADRC + BQPIO	[329.0, 337.0]	335.9	2.8	[13.0, 23.9]	17.0	3.6
	PID + BQPIO	[341.0, 351.0]	346.0	4.5	[15.3, 28.0]	19.1	7.5
Intermediate point temperature	EADRC + BQPIO	**[282.1, 364.8]**	**313.1**	**5.2**	**[2.33, 4.5]**	**2.6**	**2.1**
	ADRC + BQPIO	[314.6, 459.9]	355.7	8.7	[1.2, 9.0]	5.0	2.7
	PID + BQPIO	[370.0, 468.5]	383.1	13.4	[5.0, 18.9]	11.4	4.7

coefficient and time constant) were stochastically perturbed by±10% relative to the nominal value for the Monte Carlo random test. The number of samples is set to 200. Then, a positive step with amplitude of 10 is added into the active power channel, results are displayed in Fig. 8. Performance indicators such as the average, variable range and standard deviation (denote as *Mean*, Range and *SD*) of settling time t_s and overshoot σ% are recorded in Table 10.

The *Mean* recorded in Table 10 represents the average performance level of the USC unit based on various controllers for the perturbed model. The smaller *Mean* stand for the stronger robustness. *SD* is used to describe the discrete degree of Monte Carlo random experimental results. It can be seen from Table 10 that the average overshoot of USC unit regulated by the EADRC + BQPIO algorithm is only 21.6% while the ADRC + BQPIO and PID + BQPIO strategies are 22.5% and 22.8% in the robustness test of active power channel. Whether it is the performance indicators in Table 10 or the perfectly concentrated red point cluster depicted in Fig. 8 reveals the strongest robustness of EADRC + BQPIO.

In addition to the excellent target tracking performance, disturbance rejection capacity and robustness, the industrial practicability of the EADRC approach is also outstanding. The EADRC strategy with the fixed 1- degree-of freedom structure is convenient for discretization. And then, a various of swarm optimization algorithms can be used to deal with the parameters optimization issue of EADRC in real-time. Under these circumstances, the flexible operation of 1000 MW USC unit under full operating conditions is easy to be realized by the practical EADRC scheme.

5. Conclusions

To accelerate the transformation of low-carbon power system, a flexible EADRC scheme optimized by the BQPIO algorithm is applied to promote the flexible operation capacity of the 1000 MW USC unit under full operating conditions. As an effective reference for the flexibility problem, here are the main conclusions.

1) As the EADRC approach with remarkable control performance can be directly implemented on the existing control system, the rapid load regulation and deep peak shaving capacity of 1000 MW USC unit have been successfully improved. Benefit from this, the flexible operation of USC unit under full operating conditions can be achieved. However, only the EADRC method with the with discrete-time structure is convenient for its industrial expansion.
2) A total of 3000 tests of 5 meta-heuristic optimization algorithms were carried out based on 9 benchmark functions on CEC 2014 library. The invincible optimization accuracy and convergence speed of BQPIO algorithm are confirmed in most tests. Then, the parameters automatic tuning mechanism for EADRC is gained by the BQPIO

algorithm. Profit from that, the control performance of USC unit can always meet the flexibility requirements which is conducive to its safe and stable operation. Nevertheless, the delay between the algorithm execution and actual process should be further shortened.
3) Thanks to the remarkable control performance of EADRC+BQPIO algorithm, the average settling time for USC unit to response to load demand is reduced to 130.50s while the ADRC+BQPIOand PID+BQPIO methods respectively are 165.45s and 266.35s in the deep peak shaving process. Additionally, during the load rising process, the average load tracking error of USC unit regulated by the EADRC + BQPIO scheme decreases to 3.653 MW, which is only 71.51% and 69.06% of ADRC + BQPIO and PID + BQPIO algorithms.

The practicability of the flexible EADRC technology mainly reflected in its direct implement on the existing discrete control system without any devices modifications. However, how to quickly and accurately choose the parameters of multivariable EADRC to ensure the stability of the closed-loop control circuit still need in-depth research. In addition, the inevitable delay of output variables in USC unit also affects the rapidity of EADRC algorithm. The structuration and solution of the multi-objective optimization function in the flexible operation of thermal power unit is worth to be further discussed. In order to extend its industrial applications in thermal power unit, it is necessary to discretize the flexible EADRC algorithm. Thereby, future opportunities may involve the following trends: selecting the parameters ranges of EADRC based on theoretical analyses, exploring parameters on-online tuning method, investigating the discretization of EADRC, developing a comprehensive evaluation criterion to assess the flexible operation capacity of thermal power unit, and so on.

Credit author statement

Guolian Hou: Supervision, Reviewing and Editing, Data curation. Ting Huang: Conceptualization, Methodology, Software, Validation, Writing, Investigation. Congzhi Huang: Reviewing and Editing, Funding acquisition.

Declaration of competing interest

The authors declare that they have no known competing financial interests or personal relationships that could have appeared to influence the work reported in this paper.

Data availability

My research code needs to be kept secret

Acknowledgement

This work is supported by the National Natural Science Foundation of China (Grant No. 61973112). The anonymous reviewers' insightful comments and valuable suggestions are also greatly appreciated.

References

[1] Liu MM, Liu M, Chen WX, Yan JJ. Operational flexibility and operation optimization of CHP units supplying electricity and two-pressure steam. Energy 2023;263:125988.

[2] Xin YL, Zhao T, Chen X, He KL, Ma H, Chen Q. Heat current method-based real-time coordination of power and heat generation of multi-CHP units with flexibility retrofit. Energy 2022;252:124018.

[3] Hou GL, Gong LJ, Hu B, Huang T, Su HL, Huang CZ, Zhou GP, Wang SJ. Flexibility oriented adaptive modeling of combined heat and power plant under various heat-power coupling conditions. Energy 2022;242:122529.

[4] Fan H, Su ZG, Wang PH, Lee KW. A dynamic nonlinear model for a wide-load range operation of ultra-supercritical once-through boiler-turbine units. Energy 2021; 226:120425.

[5] Huang CZ, Sheng XX. Data-driven model identification of boiler-turbine coupled process in 1000 MW ultra-supercritical unit by improved bird swarm algorithm. Energy 2020;205:118009.

[6] Jin TY, Chen XY, Wen JY, Wu QW, Bai LQ, Liu YF, Cao Y. Improved ramping and reserve modeling of combined heat and power in integrated energy systems for better renewable integration. IEEE Trans Sustain Energy 2022;13(2):683–92.

[7] Varghese S, Dalvi S, Narula A, Webster M. The impacts of distinct flexibility enhancements on the value and dynamics of natural gas power plant operations sushant. IEEE Trans Power Syst 2021;36(6):5803–13.

[8] Wang YC, Lou SH, Wu YW, Wang SR. Flexible Operation of retrofitted coal-fired power plants to reduce wind curtailment considering thermal energy storage. IEEE Trans Power Syst 2020;35(2):1178–87.

[9] Hou GL, Xiong J, Zhou GP, Gong LJ, Huang CZ, Wang SJ. Coordinated control system modeling of ultra-supercritical unit based on a new fuzzy neural network. Energy 2021;234:121231.

[10] Hou GL, Gong LJ, Hu B, Su HL, Huang T, Huang CZ, Fan W, Zhao YZ. Application of fast adaptive moth-flame optimization in flexible operation modeling for supercritical unit. Energy 2022;239:121843.

[11] Al-Momani A, Mohamed O, Elhaija W. Multiple processes modeling and identification for a cleaner supercritical power plant via grey wolf optimizer. Energy 2022;252:124090.

[12] Zhu MJ, Liu YD, Wu X, Shen J. Dynamic modeling and comprehensive analysis of direct air-cooling coal-fired power plant integrated with carbon capture for reliable, economic and flexible operation. Energy 2023;263:125490.

[13] Zima W, Grądziel S, Cebula A, Rerak M, Kozak-Jagieła E. Mathematical model of a power boiler operation under rapid thermal load changes. Energy 2023;263: 125836.

[14] Saleh A, Nanomaterials T. Classification, properties, and environmental toxicities. Environ Technol Innovat 2020;20:101067.

[15] Ullah I, Rab A, Rahim A, Tariq M, Hassan A, Saleh T A, Khan J, Khan H. The stimulus role of lithium sulfate (Li2SO4) on the electrical and mechanical properties of poly (vinyl alcohol)-MWCNTS-based thin film composites. J Mater Sci Mater Electron 2022;33:18157–66.

[16] Khana H M, Mustaqeem M, Chen Y, Junaid M, Saleh T A, Akram M, Rehman A, Lateef N. Tuning of structural and dielectric properties of X type hexaferrite through Co and Zn variation. J Alloys Compd 2022;909:164529.

[17] Sharif A, Mustaqeem M, Saleh T A, Rehman A, Ahmad M, Warsi M. Synthesis, structural and dielectric properties of Mg/Zn ferrites-PVA nanocomposites. Mater Sci Eng B 2022;280:115689.

[18] Wang D, Liu DY, Wang CN, Zhou YL, Li XL, Yang M. Flexibility improvement method of coal-fired thermal power plant based on the multi-scale utilization of steam turbine energy storage. Energy 2022;239:122301.

[19] Zhang KZ, Zhao YL, Liu M, Gao L, Fu Y, Yan JJ. Flexibility enhancement versus thermal efficiency of coal-fired power units during the condensate throttling processes. Energy 2021;218:119534.

[20] Han ZH, Xiang P. Modeling condensate throttling to improve the load change performance of cogeneration units. Energy 2020;192:116684.

[21] Zhao YL, Wang CY, Liu M, Chong DT, Yan JJ. Improving operational flexibility by regulating extraction steam of high-pressure heaters on a 660 MW supercritical coal-fired power plant: a dynamic simulation. Appl Energy 2018;212:1295–309.

[22] Wang Z, Liu M, Zhao YL, Wang CY, Chong DT, Yan JJ. Flexibility and efficiency enhancement for double-reheat coal-fired power plants by control optimization considering boiler heat storage. Energy 2020;201:117594.

[23] Cao LH, Wang ZZ, Pang TY, Dong EF, Hu PF, Liu M, Ma TS. Analysis on wind power accommodation ability and coal consumption of heat-power decoupling technologies for CHP units. Energy 2021;231:120833.

[24] Wang CY, Song JW. Performance assessment of the novel coal-fired combined heat and power plant integrating with flexibility renovations. Energy 2022. https://doi.org/10.1016/j.energy.2022.125886.

[25] Yan H, Liu M, Wang Z, Zhang KZ, Chong DT, Yan JJ. Flexibility enhancement of solar-aided coal-fired power plant under different direct normal irradiance conditions. Energy 2023;262:125349.

[26] Zhu HY, Tan P, He ZQ, Zhang C, Fan QY, Chen G. Nonlinear model predictive control of USC boiler-turbine power units in flexible operations via input convex neural network. Energy 2022;255:124486.

[27] Wang Z, Liu M, Yan H, Yan JJ. Optimization on coordinate control strategy assisted by high-pressure extraction steam throttling to achieve flexible and efficient operation of thermal power plants. Energy 2022;244:122676.

[28] Zeng DL, Gao YK, Hu Y, Liu JZ. Optimization control for the coordinated system of an ultra-supercritical unit based on stair-like predictive control algorithm. Control Eng Pract 2019;82:185–200.

[29] Gao YK, Zeng DL, Ping BY, Zhang LX, Liu JZ. Research on coordinated control system of drum boiler units considering energy demand decoupling. Control Eng Pract 2020;102:104562.

[30] Hou GL, Gong LJ, Huang CZ, Zhang JH. Novel fuzzy modeling and energy-saving predictive control of coordinated control system in 1000 MW ultra-supercritical unit. ISA Trans 2019;86:48–61.

[31] Zhou H, Chen C, Lai JG, Lu XQ, Deng QJ, Gao XR, Lei ZC. Affine nonlinear control for an ultra-supercritical coal fired once-through boiler-turbine unit. Energy 2018; 153:638–49.

[32] Han JQ. From PID to active disturbance rejection control. IEEE Trans Ind Electron 2009;56(3):900–6.

[33] Yuan Y, Wang ZD, Yu Y, Guo L, Yang HJ. Active disturbance rejection control for a pneumatic motion platform subject to actuator saturation: an extended state observer approach. Automatica 2019;107:353–61.

[34] Wu ZL, Liu YH, Li DH, Chen YQ. Multivariable active disturbance rejection control for compression liquid chiller system. Energy 2023;262:125344.

[35] Hui JW, Yuan JQ. Load following control of a pressurized water reactor via finite-time super-twisting sliding mode and extended state observer techniques. Energy 2022;241:122836.

[36] Wu ZL, Yuan J, Liu YH, Li DH, Chen YQ. An active disturbance rejection control design with actuator rate limit compensation for the ALSTOM gasifier benchmark problem. Energy 2021;227:120447.

[37] Hou GL, Huang T, Zheng FM, Gong LJ, Huang CZ, Zhang JH. Application of multi-agent EADRC in flexible operation of combined heat and power plant considering carbon emission and economy. Energy 2023;263:125711.

[38] Huang CZ, Zhuang JN. Error-based active disturbance rejection control for pitch control of wind turbine by improved coyote optimization algorithm. IEEE Trans Energy Convers 2022;37(2):1394–405.

[39] Hou GL, Ke Y, Huang CZ. A flexible constant power generation scheme for photovoltaic system by error-based active disturbance rejection control and perturb & observe. Energy 2021;237:121646.

[40] Wu ZL, Li DH, Xue YL, Chen YQ. Gain scheduling design based on active disturbance rejection control for thermal power plant under full operating conditions. Energy 2019;185:744–62.

[41] Dong Z, Li BW, Li JY, Guo ZW, Huang XJ, Zhang YJ, Zhang ZY. Flexible control of nuclear cogeneration plants for balancing intermittent renewables. Energy 2021; 221:119906.

[42] Yang C, Wang Y, Toumi K. Hierarchical antidisturbance control of a piezoelectric stage via combined disturbance observer and error-based ADRC. IEEE Trans Ind Electron 2022;69(5):5060–70.

[43] Madonski R, Ramirez NM, Stanković M, Shao S, Gao Z, Yang J, Sun L. On vibration suppression and trajectory tracking in largely uncertain torsional system: an error-based ADRC approach. Mech Syst Signal Process 2019;134:106300.

[44] Taieb A, Salhi H, Chaari A. Adaptive TS fuzzy MPC based on particle swarm optimization-cuckoo search algorithm. ISA Trans 2022. https://doi.org/10.1016/j.isatra.2022.05.018.

[45] Basu M. Fuel constrained combined heat and power dynamic dispatch using horse herd optimization algorithm. Energy 2022;246:123396.

[46] Hou GL, Gong LJ, Yang ZL, Zhang JH. Multi-objective economic model predictive control for gas turbine system based on quantum simultaneous whale optimization algorithm. Energy Convers Manag 2020;207:112498.

[47] Liang J, Ge SL, Qu BY, Yu KJ, Liu FJ, Yang HT, Wei PP, Li ZM. Classified perturbation mutation based particle swarm optimization algorithm for parameters extraction of photovoltaic models. Energy Convers Manag 2020;203:112138.

[48] Hachana O, El-Fergany A. Efficient PEM fuel cells parameters identification using hybrid artificial bee colony differential evolution optimizer. Energy 2022;250: 123830.

[49] Duan HB, Qiao PX. Pigeon-inspired optimization: a new swarm intelligence optimizer for air robot path planning. International Journal of Intelligent Computing and Cybernetics 2014;7:23–37.

[50] Duan HB, Xin L, Shi YH. Homing pigeon-inspired autonomous navigation system for unmanned aerial vehicles. IEEE Trans Aero Electron Syst 2021;57(4):2218–24.

[51] Pan J, Tian A, Snasel V, Kong LP, Chu S. Maximum power point tracking and parameter estimation for multiple-photovoltaic arrays based on enhanced pigeon-inspired optimization with Taguchi method. Energy 2022;251:123863.

[52] Zhao ZL, Zhang MY, Zhang ZH, Wang YW, Cheng RT, Guo JT, Yang P, Lai CS, Li P, Lai LL. Hierarchical pigeon-inspired optimization-based MPPT method for photovoltaic systems under complex partial shading conditions. IEEE Trans Ind Electron 2020;69(10):10129–43.

[53] He HX, Duan HB. A multi-strategy pigeon-inspired optimization approach to active disturbance rejection control parameters tuning for vertical take-off and landing fixed-wing UAV. Chin J Aeronaut 2022;35(1):19–30.

[54] Hai XS, Wang ZL, Feng Q, Ren Y, Xu BH, Cui JJ, Duan HB. Mobile robot ADRC with an automatic parameter tuning mechanism via modified pigeon-inspired optimization. IEEE/ASME Trans Mechatronics 2019;24:2616–26.

[55] Hou GL, Gong LJ, Hu B, Huang T, Su HL, Huang CZ, Zhou GP, Wang SJ. Flexibility oriented adaptive modeling of combined heat and power plant under various heat-power coupling conditions. Energy 2022;242:122529.

[56] Madonski R, Shao S, Zhang H, Gao ZQ, Yang J, Sun L. General error-based active disturbance rejection control for swift industrial implementations. Control Eng Pract 2019;84:218–29.

[57] Liang JJ, Qu BY, Suganthan PN. Problem definitions and evaluation criteria for the CEC 2014 special session and competition on single objective real-parameter numerical optimization. Technical report. In: China and technical report, nanyang technological university. Zhengzhou,: computational intelligence laboratory, Zhengzhou university; 2013.

[58] Hou GL, Gong LJ, Huang CZ, Zhang JH. Fuzzy modeling and fast model predictive control of gas turbine system. Energy 2020;200:117465.